AN EXPANDING MANIFOLD IN TRANSMODAL REGIONS CHARACTERIZES ADOLESCENT RECONFIGURATION OF STRUCTURAL CONNECTOME ORGANIZATION

Bo-yong Park[a,b*], Richard A. I. Bethlehem[c,d], Casey Paquola[a,e], Sara Larivière[a], Raul R. Cruces[a], Reinder Vos de Wael[a], Neuroscience in Psychiatry Network (NSPN) Consortium[1] , Edward T. Bullmore[d], Boris C. Bernhardt[a*]

[a]McConnell Brain Imaging Centre, Montreal Neurological Institute and Hospital, McGill University, Montreal, Quebec, Canada; [b]Department of Data Science, Inha University, Incheon, South Korea; [c]Autism Research Centre, Department of Psychiatry, University of Cambridge, Cambridge, United Kingdom; [d]Brain Mapping Unit, Department of Psychiatry, University of Cambridge, Cambridge, United Kingdom; [e]Institute of Neuroscience and Medicine (INM-1), Forschungszentrum Jülich, Jülich, Germany

***Corresponding Authors:**

Bo-yong Park, PhD
Department of Data Science
Inha University
Incheon, South Korea
Phone: +82-32-860-9427
Email: boyong.park@inha.ac.kr

Boris C. Bernhardt, PhD
Multimodal Imaging and Connectome Analysis Lab
McConnell Brain Imaging Centre
Montreal Neurological Institute and Hospital
McGill University
Montreal, Quebec, Canada
Phone: +1-514-398-3579
Email: boris.bernhardt@mcgill.ca

[1]A complete list of investigators from the Neuroscience in Psychiatry Network (NSPN) Consortium can be found in the Supporting Information.

ABSTRACT

Adolescence is a critical time for the continued maturation of brain networks. Here, we assessed structural connectome development in a large longitudinal sample ranging from childhood to young adulthood. By projecting high-dimensional connectomes into compact manifold spaces, we identified a marked expansion of structural connectomes with the strongest effects in transmodal regions during adolescence. Findings reflected increased within-module connectivity together with increased segregation, indicating increasing differentiation of higher-order association networks from the rest of the brain. Projection of subcortico-cortical connectivity patterns into these manifolds showed parallel alterations in pathways centered on the caudate and thalamus. Connectome findings were contextualized via spatial transcriptome association analysis, highlighting genes enriched in cortex, thalamus, and striatum. Statistical learning of cortical and subcortical manifold features at baseline and their maturational change predicted measures of intelligence at follow-up. Our findings demonstrate that connectome manifold learning can bridge the conceptual and empirical gaps between macroscale network reconfigurations, microscale processes, and cognitive outcomes in adolescent development.

IMPACT:
Manifold learning of longitudinal brain network data provides novel insights into adolescent structural connectome maturation, and how multiple scales of cortical and subcortical organization interact in typical neurodevelopment.

KEYWORDS:
Connectome; neurodevelopment; adolescence; longitudinal; neuroimaging; multi-scale

INTRODUCTION

Adolescence is a time of profound and genetically mediated changes in whole-brain network organization (Larsen and Luna, 2018; Menon, 2013). Adolescent development is important for the overall maturation in cognitive and educational functions and brain health more generally, a notion reinforced by the overlapping onset of several neurodevelopmental and psychiatric disorders (Hong et al., 2019; Khundrakpam et al., 2017; Paus et al., 2008). With increased capacity to carry out longitudinal studies in large samples, it is now possible to track changes in brain network organization within subjects, providing mechanistic insights into maturational processes, their biological underpinnings, and their effects on behavior and cognition.

By offering an *in vivo* window into brain organization, neuroimaging techniques such as magnetic resonance imaging (MRI) offer the ability to track adolescent brain development over time. Early cross-sectional and longitudinal studies in neurodevelopmental cohorts focused on the analysis of morphological changes (Gogtay et al., 2004; Shaw et al., 2006; Tamnes et al., 2017), including MRI-based cortical thickness (Shaw et al., 2006; Tamnes et al., 2017) and volumetric measures (Gogtay et al., 2004; Tamnes et al., 2017). Studies robustly show initial grey matter increases until mid-late childhood followed by a decline for the rest of the lifespan. During adolescence, cortical thickness decreases in widespread brain regions (Khundrakpam et al., 2013; Shaw et al., 2006; Sotiras et al., 2017; Tamnes et al., 2017). Thus, contextualizing connectome alterations relative to established patterns of cortical thickness findings may establish whether inter-regional network changes occur above and beyond these diffuse effects of regional morphological maturation. More recent work explored changes in intracortical microstructure, capitalizing on myelin-sensitive contrasts such as magnetization transfer ratio (MT) mapping, which generally suggest overall increases in adolescence (Paquola et al., 2019a; Whitaker et al., 2016) together with depth-dependent shifts in intracortical myelin profiles (Paquola et al., 2019a). Besides the increasingly recognized changes in cortico-cortical connectivity, additionally studying subcortical regions offer additional insights for understanding brain maturation during adolescence. Indeed, an increasing body of connectome level studies emphasizes that subcortical structures contribute significantly to patterns of whole-brain organization, dynamics, and cognition (Hwang et al., 2017; Müller et al., 2020; Shine et al., 2019). In prior neurodevelopmental studies, it has been shown that the volumes of the striatum and thalamus decrease between adolescence and adulthood, potentially paralleling processes resulting in cortical grey matter reduction during this time window (Herting et al., 2018). A close inter-relationship between cortical and subcortical development is also suggested by recent functional connectivity work suggesting that cortico-subcortical pathways are intrinsically remodeled during adolescence (Váša et al., 2020), and these changes affect cognitive functioning. Collectively, these prior findings suggest measurable trajectories of cortical and subcortical structural organization and support associations to cognitive development (Baum et al., 2020; Shaw et al., 2006).

Recent conceptual and methodological advances enable the study of brain organization, development, and substrates underlying cognitive trajectories in humans. One key modality to track developmental changes in structural connectivity is diffusion MRI (dMRI), a technique sensitive to the displacement of water in tissue that allows for the non-invasive approximation of inter-regional white matter tracts. Prior cross-sectional and longitudinal studies in children and adolescents outlined changes in the microstructure of major white matter tracts during development based on the analysis of dMRI derived tissue parameters (Lebel and Beaulieu, 2011; Schmithorst and Yuan, 2010). These findings have been complemented by assessments of brain network topology using graph-theoretical analysis (Baker et al., 2015; Hagmann et al., 2010; Lebel and Beaulieu, 2011; Oldham and Fornito, 2019), which reported a relatively preserved spatial layout of structural hubs across adolescent development on the one hand (Hagmann et al., 2010), yet with a continued strengthening of their connectivity profiles, likely underpinned by the ongoing maturation of long-range association fibers (Baker et al., 2015; Lebel and Beaulieu, 2011; Oldham and Fornito, 2019).

One emerging approach to address connectome organization and development comes from the application of manifold learning techniques to connectivity datasets. By decomposing whole-brain structural and functional connectomes into a series of lower dimensional axes capturing spatial gradients of connectivity variations, these techniques provide a compact perspective on large-scale connectome organization (Margulies et al., 2016; Paquola et al., 2019b; Vos de Wael et al., 2020). In addition, these techniques capture multiple, potentially overlapping gradients in connectivity along cortical mantle, which can represent both subregional heterogeneity and multiplicity within a brain region (Haak and Beckmann, 2020). In prior work, we showed that multiple dMRI gradients can illustrate structural underpinnings of dynamic functional communication in the adult human connectome (Park et al., 2021). In line with prior conceptual accounts, the low-dimensional eigenvectors (*i.e.,* gradients) derived from these techniques provide continuous dimensions of cortical organization, and thus the eigenvectors can jointly generate intrinsic coordinate systems of the brain based on connectivity (Bijsterbosch et al., 2020; Haak et al., 2018; Huntenburg et al., 2018; Margulies et al., 2016; Mars et al., 2018). Beyond these methodological considerations, prior work has shown that the principal gradients estimated from resting-state functional (Margulies et al., 2016), microstructural (Paquola et al., 2019b), and diffusion MRI (Park et al., 2020a) all converge broadly along an established model of sensory-fugal hierarchy and laminar differentiation (Mesulam, 1998), allowing gradient mapping techniques to make conceptual contact to theories of cortical organization, development, and evolution (Buckner and Krienen, 2013; Goulas et al., 2018; Huntenburg et al., 2018; Sanides, 1969, 1962). An emerging literature has indeed shown utility of the gradient framework to study primate evolution and cross-species alignment (Blazquez Freches et al., 2020; Sofie L. Valk et al., 2020; T. Xu et al., 2020), neurodevelopment (Hong et al., 2019; Paquola et al., 2019a), as well as plasticity and structure-function coupling (Park et al., 2021; Sofie L Valk et al., 2020; Vázquez-Rodríguez et al., 2019). In a recent assessment by our team, manifold learning techniques have been applied to myelin sensitive intracortical MT data, showing an increasing myeloarchitectural differentiation of association cortex throughout adolescence (Paquola et al., 2019a). Still, the longitudinal maturation of dMRI connectomes in children and adolescents using manifold techniques has not been tracked.

Imaging-transcriptomics approaches allow for the identification of cellular and molecular factors that co-vary with imaging-based findings (Arnatkeviciute et al., 2019; Fornito et al., 2019; Gorgolewski et al., 2014; Hawrylycz et al., 2015; Thompson et al., 2013). Recently established resources, such as the Allen Human Brain Atlas (Arnatkeviciute et al., 2019; Hawrylycz et al., 2015), can be utilized to spatially associate macroscale imaging/connectome data with the expression patterns of thousands of genes. These findings have already been applied in the study of healthy adults (Hawrylycz et al., 2015; Park et al., 2020b; Q. Xu et al., 2020) and typically developing adolescents (Mascarell Maričić et al., 2020; Padmanabhan and Luna, 2014; Paquola et al., 2019a; Vértes et al., 2016; Whitaker et al., 2016), as well as individuals suffering from prevalent brain disorders (Altmann et al., 2018; Hashimoto et al., 2015; Klein et al., 2017; Park et al., 2020a; Patel et al., 2021; Romero-Garcia et al., 2019). The gene sets that co-vary with *in vivo* findings can furthermore be subjected to gene set enrichment analyses to discover potentially implicated molecular, cellular, and pathological processes (Ashburner et al., 2000; Carbon et al., 2019; Chen et al., 2013; Dougherty et al., 2010; Kuleshov et al., 2016; Morgan et al., 2019; Romero-Garcia et al., 2018; Subramanian et al., 2005). For example, studies in newborns have shown that cortical morphology reflects spatiotemporal patterns of gene expression in foetuses, linking molecular mechanisms to *in vivo* measures of cortical development in early life (Ball et al., 2020). Work in adolescents has furthermore shown that developmental changes in regional cortical thickness measures and myelin proxies spatially co-localize with the expression patterns of genes involved in synaptic and oligodendroglial function (Paquola et al., 2019a; Whitaker et al., 2016). Building on these prior investigations, the current study aimed at exploring whether adolescent structural connectome reconfigurations, assessed using manifold learning techniques, reflect the expression patterns of specific genes, in order to identify potential molecular signatures of macroscale structural network development.

Here, we charted developmental changes in structural connectome organization, based on an accelerated longitudinal neuroimaging study involving 208 participants investigated between 14 to 26 years of age (Kiddle et al., 2018; Whitaker et al., 2016). Compared to cross-sectional designs, longitudinal studies track within-subject change, separating developmental effects from between-subject variability (Louis et al., 1986). We first estimated longitudinal changes in structural connectome manifolds across age. This compact and lower dimensional space furthermore allowed for the integration of connectome level findings with changes in MRI-based measures of cortical morphology and intracortical myelin. We furthermore projected subcortico-cortical connectivity patterns into the manifold space, to assess parallel developmental shifts of these pathways in the studied time window. Connectome-manifold changes were contextualized at the molecular level via transcriptomic association and developmental enrichment analyses based on *post-mortem* datasets, which furthermore allowed for data-driven exploration of time windows of spatially co-localized gene sets. To also assess behavioral associations of connectome manifold changes, we utilized supervised machine learning to predict future measures of cognitive function quantified via the intelligence quotient (IQ). IQ is a widely used marker of general cognitive abilities, which shows good test-retest reliability (Brown and May, 1979; Canivez and Watkins, 1998; Catron, 1978; Matarazzo et al., 1973; Snow et al., 1989; Wagner and Caldwell, 1979) and has previously been applied to index overall cognitive function during development (Crespi, 2016; Garde et al., 2005, 2000; Koenis et al., 2018; Park et al., 2016; Ramsden et al., 2011; Shaw et al., 2006; Suprano et al., 2020). In the study of neurodevelopment, neuroimaging reports have previously assessed associations between IQ and large-scale network measures in children to adolescents (Koenis et al., 2018; Ramsden et al., 2011; Seidlitz et al., 2018; Shaw et al., 2006; Suprano et al., 2020). Multiple sensitivity analyses were conducted at several steps to verify the robustness of our findings, and analytical code is made fully accessible to allow for independent replication of our findings.

RESULTS

These findings were based on the Neuroscience in Psychiatry Network (NSPN) cohort (Kiddle et al., 2018; Whitaker et al., 2016). In brief, we studied 208 healthy individuals enrolled in an accelerated longitudinal study, with approximately equal numbers of males and females in each of five age-related strata that collectively spanned the time period from 14 to 25 years coinciding with transition from adolescence to young adulthood. Participants (48% female) had a mean age of 18.82 years (range = 14–25 years) at baseline and 19.95 years (15–26 years) at follow-up. The average interval between baseline and follow-up scan was 11.28 months (range = 6–12 months). See *Methods* for details on participant selection, image processing, and analysis.

Macroscale structural connectome manifold

For every participant, we built cortex-wide structural connectome manifolds formed by the eigenvectors displaying spatial gradients in structural connectome organization using non-linear dimensionality reduction techniques (https://github.com/MICA-MNI/BrainSpace) (Vos de Wael et al., 2020). Individual manifolds were aligned to a template manifold estimated from a hold-out dataset (see *Methods*) (Langs et al., 2015; Vos de Wael et al., 2020). Three eigenvectors (E1, E2, and E3) explained approximately 50% of information in the template affinity matrix (*i.e.,* 20.7/15.8/13.5% for E1/E2/E3, respectively), with each eigenvector showing a different axis of spatial variation across the cortical mantle (**Fig. 1A**). Eigenvectors depicted a continuous differentiation between medial and lateral cortices (E1), between inferior and superior cortices (E2), and between anterior and posterior areas (E3). For each participant and time point, we calculated *manifold eccentricity*, which depicts how far each node is located from the center of the template manifold (see *Methods*). It thus quantifies

the changes in eigenvectors between the time points in terms of expansion and contraction instead of comparing multi-dimensional connectome manifolds (Bethlehem et al., 2020). The manifold eccentricity showed high values in frontal and somatomotor regions, while temporoparietal, visual, and limbic regions showed low values (**Fig. 1B**).

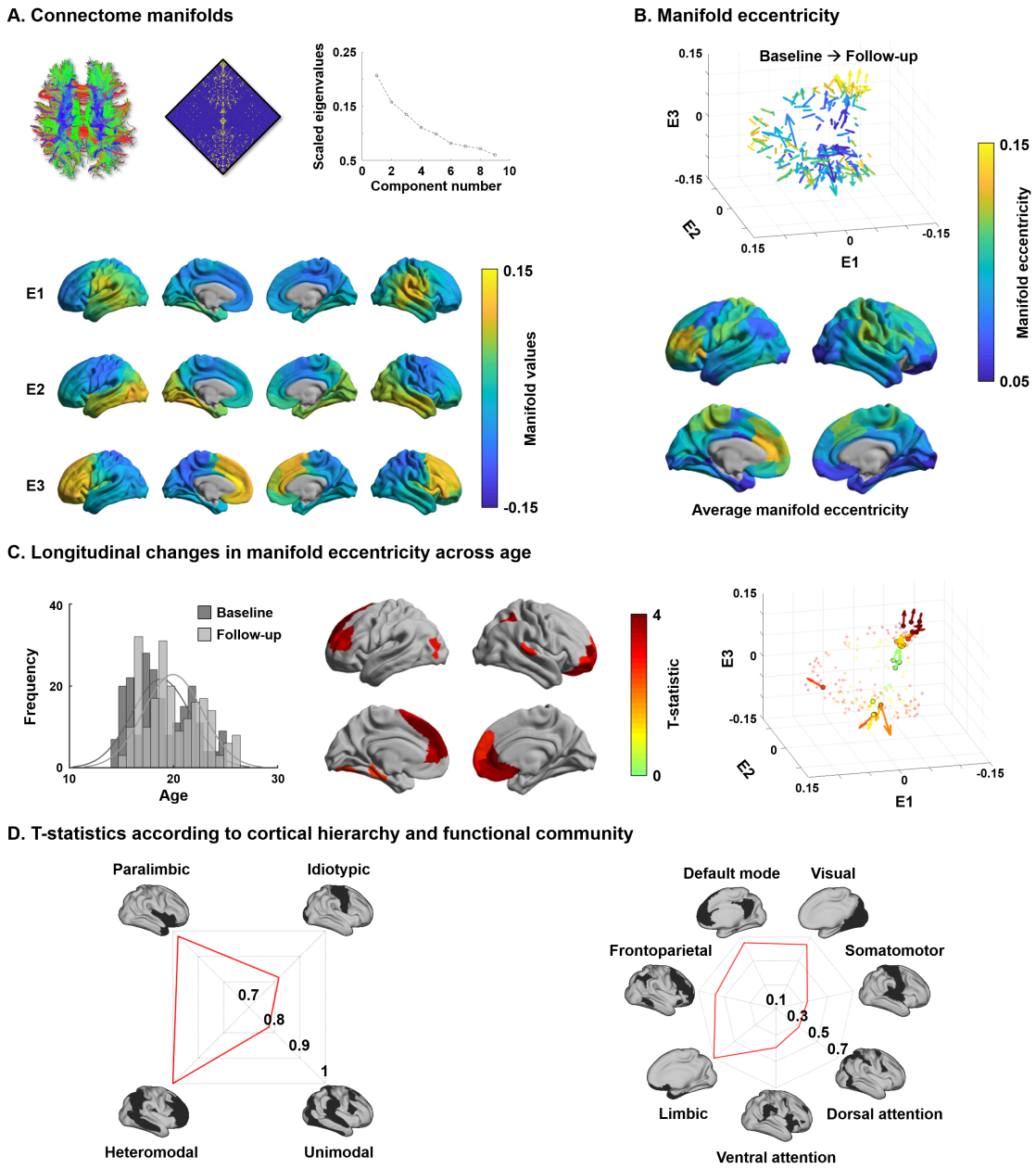

Fig. 1 | Structural connectome manifolds. (A) Systematic fiber tracking based on dMRI generated a cortex-wide structural connectome, which was subjected to diffusion map embedding. As shown in the scree plot, three eigenvectors (E1, E2, E3) accounted for approximately 50% information of connectome data, and each depicted a different gradual transition across the cortical mantle. **(B)** Manifold eccentricity measured by Euclidean distance between the template center and each data point. Arrows depict average positional change in connectivity space from baseline to follow-up. The color of each arrow represents each brain region mapped on the surface on the bottom. **(C)** The histogram represents age distribution of all subjects at baseline and follow-up. The colors on brain surfaces indicate t-statistics of regions showing significant longitudinal changes in manifold eccentricity across age, following multiple comparisons correction with a false discovery rate (FDR) < 0.05. Datapoint colors in the scatter plot represent t-statistics. Identified regions are represented with arrows that originate from baseline to follow-up. **(D)** Stratification of age-related changes in manifold eccentricity according to prior models of cortical hierarchy (Mesulam, 1998) and functional MRI communities (Yeo et al., 2011).

Changes in manifold eccentricity across age

Leveraging linear mixed effect models that additionally controlled for effects of sex, site, head motion, and subject-specific random intercepts (Worsley et al., 2009), we assessed changes in manifold eccentricity across age (see *Methods*). Manifold eccentricity expanded as age increased, especially in bilateral prefrontal and temporal areas, as well as left early visual and right lateral parietal cortices (false discovery rate (FDR) < 0.05 (Benjamini and Hochberg, 1995); **Fig. 1C**). Stratifying these effects along four cortical hierarchical levels, defined using an established taxonomy based on patterns of laminar differentiation and tract-tracing data in non-human primates (Mesulam, 1998), we identified peak effects in heteromodal association and paralimbic areas (**Fig. 1D**). Convergent findings were observed when analyzing the effects with respect to intrinsic functional communities (Yeo et al., 2011), showing highest effects in default mode and limbic areas followed by visual and frontoparietal cortices. No significant contraction of manifold eccentricity was observed. In addition, we could not find any significant effects when we fitted the model with a quadratic form of age (*i.e.,* age^2), indicating the manifold eccentricity linearly increases across age.

To conceptualize the findings derived from manifold eccentricity with respect to conventional network topologies, we correlated manifold eccentricity changes with several graph-theoretical measures of structural connectome (**Fig. S1**) (Rubinov and Sporns, 2010). We first defined six spatially contiguous clusters within the regions that showed significant age-related changes in manifold eccentricity (see *Fig. 1C*) and correlated within-subject changes in manifold eccentricity with developmental changes in degree centrality, connectivity distance, and modular parameters (*i.e.,* within-module degree and participation coefficient based on modules defined via Louvain's community detection algorithm (Blondel et al., 2008); see *Methods*; **Fig. S2**). We found significant positive associations for degree centrality and within-module degree, suggesting that connectome manifold expansion reflects a concurrent increase of overall connectivity, particularly within modules. Stratifying changes in manifold eccentricity, as well as connectome topology measures, according to the discretized age bins confirmed these age-related trends (**Fig. S3**). Indeed, except for participation coefficient, values in general increased from childhood to young adulthood.

Effects of cortical morphology and microstructure

Previous studies demonstrated significant changes in cortical morphology and microstructure during adolescence, showing co-occurring reductions in cortical thickness and MT skewness, the latter being an index of depth-dependent intracortical myelin changes in multiple lobes (Gogtay et al., 2004; Khundrakpam et al., 2017; Paquola et al., 2019a; Shaw et al., 2006). We replicated these findings by showing cortical thinning in almost all brain regions across the studied age window as well as reductions in depth-dependent MT skewness, suggestive of supragranular enrichment of myelin (**Fig. 2A**). To evaluate whether the age-related changes in manifold eccentricity were robust above and beyond these regional changes in cortical thickness and MT, we implemented linear mixed effect models including cortical thickness and MT as covariates in the analysis of developmental change in manifold eccentricity (**Fig. 2B**). While we observed virtually identical spatial patterns of manifold eccentricity changes in models that controlled for thickness, MT skewness, and both, age-related effects in regions of significant manifold eccentricity findings (see *Fig. 1C*) were reduced in models that additionally controlled for these covariates (average reduction of t-value in models controlling for thickness/MT skewness/both = 42/18/68%).

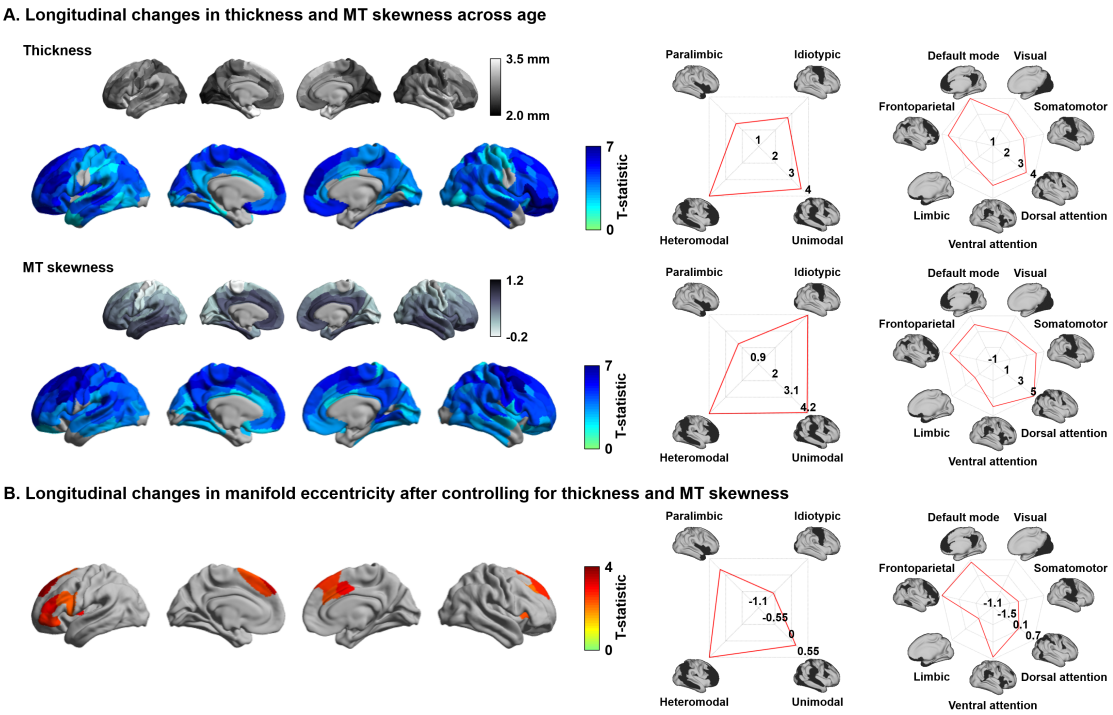

Fig. 2 | Age-related effects on macro and microstructural metrics of cortical anatomy. (A) The t-statistics of identified regions that showed significant age-related changes in cortical thickness (upper row) and MT (bottom row), and stratification of t-statistics according to cortical hierarchy (Mesulam, 1998) and functional community (Yeo et al., 2011). **(B)** Age-related changes in manifold eccentricity after controlling for cortical thickness and MT.

Age-related changes in subcortico-cortical connectivity

Besides visualizing these changes in cortico-cortical connectivity, we also capitalized on the manifold representation to assess adolescent changes in the connectivity of subcortical regions, to obtain a more holistic insight into whole-brain connectome reconfigurations during this time period, and to examine whether subcortical connectivity patterns undergo parallel developmental trajectories (Hwang et al., 2017; Shine et al., 2019). Specifically, we assessed changes in subcortical-weighted manifolds across age, defined by projecting the streamline strength of subcortical regions to cortical targets to the manifold space (see *Methods*). Such an analysis situates changes in subcortico-cortical pathways in the macroscale context of cortico-cortical connectivity identified in the previous analyses. After multiple comparisons correction, the caudate and thalamus showed significant age-related effects on subcortical-weighted manifolds (FDR < 0.05; **Fig. 3**), and marginal effects were observed in the putamen, pallidum, and hippocampus (FDR < 0.1).

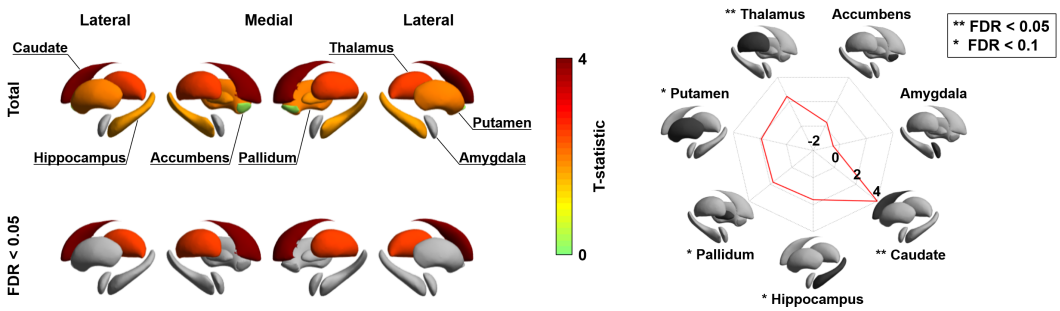

Fig. 3 | Longitudinal changes in subcortical-weighted manifolds. The t-statistics of age-related changes in subcortical-weighted manifolds. The effects of each subcortical region are reported on the radar plot. *Abbreviation:* FDR, false discovery rate.

Transcriptomic association analysis

Connectome organization in general, and macroscale gradients in particular, have been argued to reflect genetic expression profiles, underscoring the close link between the physical layout of the brain and innate transcriptional patterning (Buckner and Krienen, 2013; Fornito et al., 2019). Here, we carried out a transcriptomic association analysis and developmental enrichment analyses to contextualize the age-related manifold eccentricity changes with respect to patterns of *post-mortem* gene expression from a sample of independent adults (**Fig. 4A**). Specifically, leveraging mixed effect models, we associated the spatial patterns of manifold change across age in the NSPN sample (controlling for covariation of cortical thickness and MT) with cortical maps of *post-mortem* gene expression data from the Allen Institute for Brain Sciences (Arnatkeviciute et al., 2019; Gorgolewski et al., 2015, 2014; Hawrylycz et al., 2012; Markello et al., 2020). Among the list of most strongly associated genes (FDR < 0.05), we selected only genes that were consistently expressed across different donors (r > 0.5) (Arnatkeviciute et al., 2019; Hawrylycz et al., 2012; Markello et al., 2020) (**Data S1**). We performed developmental gene set enrichment analysis using the cell-type specific expression analysis (CSEA) tool, which compares the selected gene list with developmental enrichment profiles (see *Methods*) (Dougherty et al., 2010; Xu et al., 2014). This analysis highlights developmental time windows across macroscopic brain regions in which genes are strongly expressed. We found marked expression of the genes enriched from childhood onwards in the cortex, thalamus, and cerebellum (FDR < 0.001; **Fig. 4B**). Although signal was reduced, genes were also enriched for expression in the striatum at the transition from childhood to adolescence (FDR < 0.05). On the other hand, identified genes were not found to be expressed in the hippocampus and amygdala.

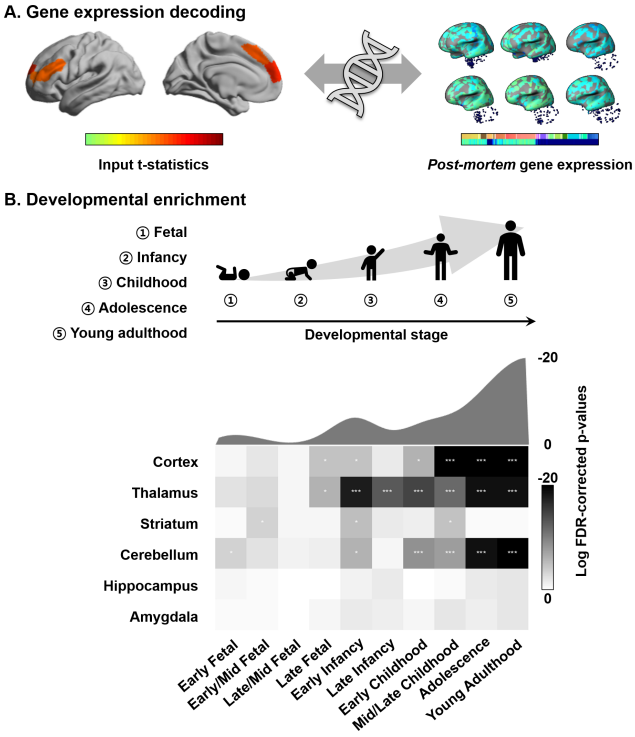

Fig. 4 | Transcriptomic analysis. (A) Gene decoding process by associating t-statistics from the linear mixed effect model with *post-mortem* gene expression maps. **(B)** We identified genes that were spatially correlated with the input t-statistic map (false discovery rate (FDR) < 0.05) and selected only those that were furthermore consistently expressed across different donors (r > 0.5). These genes were input to a developmental enrichment analysis, showing strong associations with cortex, thalamus, striatum, and cerebellum during the childhood-to-adulthood time window. The degree of gene expression for developmental windows is reported on the bottom. The curve represents log transformed FDR corrected p-values, averaged across the brain regions for each of the time windows reported on the bottom. ***FDR < 0.001, ** FDR < 0.01, *FDR < 0.05.

Association between connectome manifold and cognitive function

Finally, to establish associations between connectome reconfigurations and cognitive functioning, we utilized supervised machine learning to predict full IQ at follow-up using manifold eccentricity features. Independent variables were combinations of cortical and subcortical manifold features at baseline and their age-related trajectory data. We used elastic net regularization with nested ten-fold cross-validation (Cawley and Talbot, 2010; Parvandeh et al., 2020; Tenenbaum et al., 2000; Varma and Simon, 2006; Zou and Hastie, 2005) (see *Methods*), and repeated the prediction 100 times with different training and test dataset compositions to mitigate subject selection bias. Across cross-validation and iterations, 6.24 ± 5.74 (mean ± SD) features were selected to predict IQ using manifold eccentricity of cortical regions at baseline, 6.20 ± 5.14 cortical features at baseline and maturational change, 5.45 ± 5.99 cortical and subcortical features at baseline, and 5.16 ± 5.43 at baseline and maturational change, suggesting that adding more independent variables may not per se lead to improvement in prediction accuracy. The manifold eccentricity of cortical regions at baseline significantly predicted future IQ score (mean ± SD r = 0.14 ± 0.04; mean absolute error (MAE) = 8.93 ± 0.16, p = 0.09). Prediction performance was slightly improved when we combined the manifold eccentricity both at baseline and differences between follow-up and baseline (r = 0.18 ± 0.04; MAE = 9.10 ± 0.19, p = 0.04) (**Fig. 5A**). Notably, prediction accuracy was improved if we additionally considered subcortical manifold features (baseline: r = 0.17 ± 0.03; MAE = 8.74 ± 0.11, p = 0.04; baseline and maturational change: r = 0.21 ± 0.02; MAE = 8.86 ± 0.14, p = 0.01) (**Fig. 5B**). The regions showing strongest predictive validity for IQ were prefrontal, parietal, and temporal cortices, as well as the caudate and thalamus. The probability map of the selected brain regions (bottom right of *Fig. 5B*) was further decoded using Neurosynth (Yarkoni et al., 2011), revealing strong associations with higher order cognitive and social terms (**Fig. S4**). We compared the prediction performance of our model with a baseline model, where IQ of the test set was simple average of training set (r = -0.15 ± 0.06, MAE = 8.98 ± 0.04, p = 0.12; see *Methods*). We found that our model outperformed this baseline model (Meng's z-test p < 0.001) (Meng et al., 1992). We also predicted the change of IQ between the baseline and follow-up, instead of IQ at follow-up, using the imaging features. However, we could not find significant results.

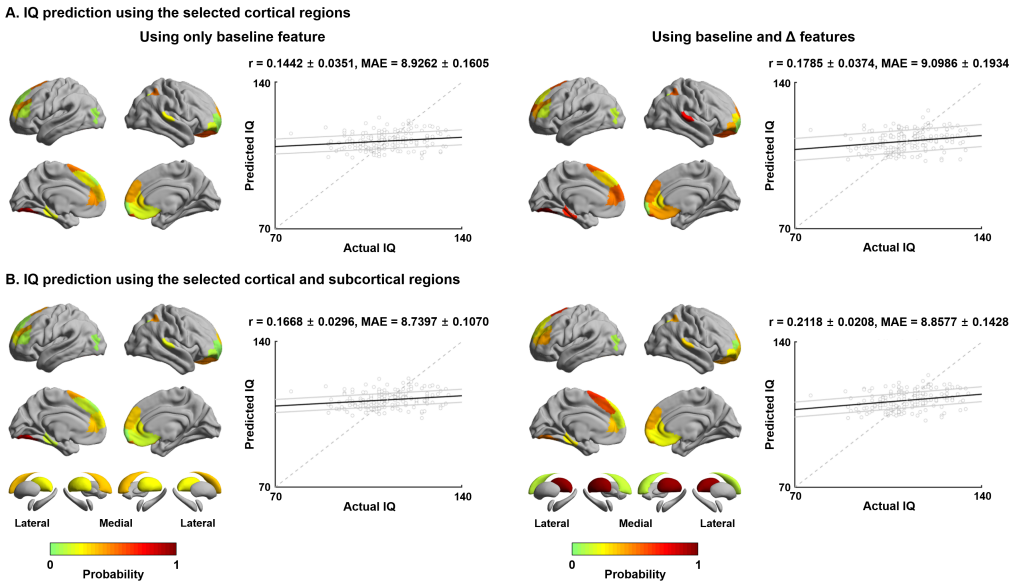

Fig. 5 | IQ prediction by baseline and follow-up measures of cortical and subcortical manifolds. (A) Probability of selected brain regions across ten-fold cross-validation and 100 repetitions for predicting future IQ using only baseline manifold eccentricity (left), and both baseline and maturational change in the feature (right). Correlations between actual and predicted IQ are reported. Black lines indicate mean correlation and gray lines represent 95% confidence interval for 100 iterations with different training/test dataset. **(B)** The prediction performance when both cortical and subcortical features were considered. *Abbreviations:* IQ, intelligence quotient; MAE, mean absolute error.

<u>Sensitivity analysis</u>

a) Spatial scale. Repeating the longitudinal modeling with a different spatial scale (*i.e.,* 300 parcels), findings were highly consistent (**Fig. S5**).

b) Site and sex effects. Furthermore, manifold eccentricity of the identified cortical regions and age consistently correlated positively across different sites and within both biological sexes, yielding non-significant interaction effects (**Fig. S6**).

c) Different parameters for diffusion map embedding. When we changed parameters of diffusion map embedding for generating connectome manifolds (see *Methods*), t-statistic maps of age-related changes in manifold eccentricity were largely consistent (mean ± SD linear correlation r = 0.92 ± 0.10).

d) Gradient alignment fidelity. When calculating linear correlations between template and individual manifolds before and after alignment, we found significant increases after alignment (r = 0.92±0.03/0.93±0.03/0.94±0.03) compared to before alignment (-0.02±0.03/-0.001±0.37/0.003±0.12), for E1/E2/E3, respectively, supporting effectiveness of alignment. After excluding 10% of subjects with poor alignment (cutoff r = 0.83; the new set was correlated with the template manifold, r= 0.94 ± 0.01), we found consistent age-related changes in manifold eccentricity (**Fig. S7**), with the t-statistic map showing strong correlation to the map derived in the whole sample (r = 0.97, p < 0.001).

e) Connectome manifold generation using principal component analysis. In a separate analysis, we generated eigenvectors using principal component analysis (Wold et al., 1987), instead of diffusion map embedding (Coifman and Lafon, 2006), and found consistent spatial maps (linear correlation = 0.998 ± 0.001 across E1/E2/E3; **Fig. S8A**) and longitudinal findings (**Fig. S8B)**.

f) Longitudinal changes in graph-theoretical measures. Repeating the longitudinal modeling using graph-theoretical centrality measures, we found significant age-related longitudinal changes in degree and eigenvector centrality, while betweenness centrality did not reveal significant effects, in similar regions to those that had significant age-related changes in manifold eccentricity (**Fig. S9**). Correlating the effect size maps for manifold eccentricity and each graph measure, we found a significant yet variable spatial similarity of the effect maps (betweenness centrality: r = 0.18, spin-test p = 0.02; degree centrality: r = 0.57, p < 0.001; eigenvector centrality: r = 0.47, p < 0.001).

g) Manifold eccentricity based on all eigenvectors. Repeating manifold eccentricity calculation and age modeling using all eigenvectors, instead of using only the first three, we observed relatively consistent results with our original findings (linear correlation of manifold eccentricity r = 0.54, p < 0.001; t-statistic map r = 0.68, p < 0.001), also pointing to manifold expansion in transmodal cortices (**Fig. S10**).

h) Robustness of group representative structural connectome. We compared gradients derived from the group representative structural connectome, based on (i) distance-dependent thresholding (Betzel et al., 2019) and (ii) consistency thresholding (Wang et al., 2019) (**Fig. S11**). We found high similarity in spatial maps of the estimated manifolds (r = 0.89 ± 0.01 for E1; 0.93 ± 0.004 for E2; 0.85 ± 0.01 for E3 across six different thresholds), indicating robustness.

i) Connectome manifolds based on structural parcellation. We repeated our analyses with a structural parcellation, defined using a sub-parcellation of folding based on the Desikan-Killiany atlas (Desikan et al., 2006; Vos de Wael et al., 2020) (**Fig. S12**). Despite slight differences in the topography of manifold eccentricity in lateral prefrontal, temporal, and occipital cortices, we could replicate strong age-related effects in heteromodal association areas, together with effects in caudate and hippocampus (FDR < 0.05), and marginally in thalamus (FDR < 0.1).

j) Longitudinal modeling using edge weights. Repeating the longitudinal modeling across age using

connectome edge weights, we found significant increases in edge weights within frontoparietal and default mode networks, as well as in attention and sensory networks (FDR < 0.05; **Fig. S13**), consistent with findings based on manifold eccentricity.

k) Manifold eccentricity and pubertal stages. We repeated the longitudinal modeling within a subset of participants who completed the Tanner scale (n = 73) (Marshall and Tanner, 1970, 1969), and found relatively consistent albeit weaker age-related changes in manifold eccentricity as for the overall sample (**Fig. S14A**). Notably, manifold eccentricity within the identified regions derived from overall sample and Tanner scale revealed a significant interaction effect (t = 2.36, p = 0.01; **Fig. S14B**), suggesting participants in early pubertal stages show more marked changes in manifold eccentricity across age compared to those in later stages.

l) IQ prediction using non-linear model. We predicted IQ at follow-up using a regression tree method (Breiman et al., 1984), instead of linear regression model, but we could not find improved prediction performance (**Fig. S15**).

DISCUSSION

The current study tracked whole-brain structural connectome maturation from adolescence to young adulthood in an accelerated longitudinal imaging cohort (Kiddle et al., 2018; Whitaker et al., 2016). Capitalizing on advanced manifold learning techniques applied to diffusion MRI derived connectomes, we established that higher order association cortices in prefrontal, medial and superior temporal areas, as well as parieto-occipital regions, expanded in their connectome manifold representation indicative of an increased differentiation of these systems from the rest of the brain in adolescence. Parallel topological analysis based on graph theory indicated that these changes anatomically coincided with increases in the within-module connectivity of transmodal cortices. Findings were consistent across the different acquisition sites and biological sexes, and similar albeit slightly weaker when correcting connectivity manifolds for MRI-based measures of macrostructure (cortical thickness) and microstructure (skewness of MT depth profile). In addition to the cortical manifold expansion, we found parallel reconfigurations of subcortical connectivity patterns for the caudate and thalamus. Decoding our findings with *post-mortem* gene expression maps implicated genes enriched in adolescence and young adulthood, again pointing to both cortical as well as subcortical targets. Finally, the combination of both cortical and subcortical manifold measures predicted behavioral measures of intelligence at follow-up, with higher performance than cortical or subcortical data alone. Collectively, our findings provide new insights into adolescent structural connectome maturation, and indicate how multiple scales of cortical and subcortical organization can interact in typical neurodevelopment.

Leveraging advanced manifold learning, we depicted macroscale connectome organization along continuous cortical axes. Similar approaches have previously been harnessed to decompose microstructural (Paquola et al., 2019b, 2019a) and functional MRI (Bethlehem et al., 2020; Hong et al., 2019; Margulies et al., 2016; Murphy et al., 2019; Vos de Wael et al., 2020). These techniques are appealing, as they offer a low dimensional perspective on connectome reconfigurations in a data-driven and spatially unconstrained manner. In our longitudinal study, we could identify marked connectome expansion during adolescence, mainly encompassing transmodal and heteromodal association cortex in prefrontal, temporal, and posterior regions, the territories known to mature later in development (Gogtay et al., 2004; Shaw et al., 2006). Findings remained consistent when we considered a linear dimensionality reduction technique, suggesting robustness to methodological details of this analysis. Connectome expansion can be understood as an overall greater differentiation

of the connectivity of these areas from the rest of the brain, as they would then cover wider portions of the corresponding manifold space. Manifold expansion in higher order areas correlated with an increase in their within-module connectivity, but not with participation coefficient and connectivity distance measures that would be more reflective of their between-module connectivity. In light of potential limitations of diffusion MRI tractography in detecting long distance fiber tracts (Betzel et al., 2019; Maier-Hein et al., 2017), we cannot rule out a reduced sensitivity of our approach for the study of long-range inter-regional connections. Nevertheless, our diffusion modelling was based on constrained spherical-deconvolution approaches together with SIFT2-based tractogram filtering, in addition to using a distance dependent thresholding approach that may have partially mitigated these limitations (Betzel et al., 2019). Thus, our findings do overall confirm and extend prior dMRI studies that have focused on specific tracts and that have indicated considerable developmental shifts in diffusion parameters, such as increases in fractional anisotropy and decreases in mean diffusivity in early and late adolescence (Olson et al., 2009). Other studies have furthermore reported increased streamline count estimates (Genc et al., 2020). In this context, our macroscale manifold findings likely reflect an ongoing consolidation of transmodal cortical communities. These findings align with prior graph-theoretical studies, which have pointed to concurrent increases in network integration and consolidation of network hubs from late childhood to early adulthood (Baker et al., 2015; Lebel and Beaulieu, 2011; Oldham and Fornito, 2019). Considering their distributed regional substrate, these network effects are likely driven by the ongoing maturation of fiber bundles that interconnect these higher order cortices, including superior longitudinal fascicules, but also thalamic and basal ganglia pathways (Tamnes et al., 2010), throughout adolescence.

Projecting manifold solutions back onto cortical surfaces allowed us to integrate our connectome manifold results with morphometric and intracortical intensity indices obtained via structural and quantitative MRI contrasts in the same participants. We were thus able to balance the network level effects against trajectories of intracortical remodeling. Longitudinal changes in these cortical features were overall in agreement with prior work, suggesting marked reductions in cortical thickness in adolescence (Khundrakpam et al., 2017; Shaw et al., 2006), possibly reflecting synaptic pruning processes (Petanjek et al., 2011) together with decreases in the skewness of intracortical MT profiles, a feature sensitive to preferential myelination of supragranular layers (Paquola et al., 2019a). Although we still observed significant age-related changes in manifold eccentricity after controlling for these intracortical and morphological measures, the effect sizes of our findings were reduced. This effect was particularly evident when running a parallel analysis that additionally controlled for depth-dependent shifts in cortical microstructure, a finding in line with more generally demonstrated links between cortical microstructural depth profiles and inter-regional connectivity (Paquola et al., 2019b). In the context of adolescence and prior findings in the NSPN dataset (Paquola et al., 2019a), these results thus suggest a coupled process that affects depth-dependent shifts in cortical myeloarchitecture on the one hand, and adolescent shifts in macroscale connectome organization on the other hand, as shown by our longitudinal manifold analyses.

In addition to emphasizing a distributed set of association cortices and their cortico-cortical connections, analysis of subcortico-cortical connectivity patterns highlighted parallel developmental processes in several subcortical structures and their connections, particularly the caudate and thalamus. These findings were independently supported by transcriptomic association studies and developmental enrichment analyses, which implicated genes expressed in cortical regions and these subcortical structures during late childhood, adolescence, and young adulthood. The caudate nucleus of the striatum has long been recognized to play an important role in mediating large-scale cortical network organization (Aglioti, 1997; Alexander and Crutcher, 1990; Graybiel, 1995), a finding also

increasingly recognized in the connectome literature (Hwang et al., 2017; Müller et al., 2020; Shine et al., 2019). It is known to modulate activity in prefrontal association areas during memory-driven internal thought processes (Aglioti, 1997), and higher order cognitive functions, notably motivational processes, decision making, as well as cognitive control and executive functions more generally (Aglioti, 1997; Graybiel, 1995). Regions of the striatum participate in dense cortico-subcortical feedback loops, and exchanges neural activity through dense connections with adjacent basal ganglia structures as well as the thalamus (Aglioti, 1997; Alexander and Crutcher, 1990; Shine, 2021). Associating macroscopic changes in manifold eccentricity with *post-mortem* microarray data provided by the Allen Human Brain Atlas (Arnatkeviciute et al., 2019; Fornito et al., 2019; Gorgolewski et al., 2014; Hawrylycz et al., 2015; Thompson et al., 2013), we identified gene sets expressed in cortical regions and subcortical structures of the thalamus and striatum during late childhood, adolescence, and young adulthood. Despite these findings being associative and based on separate datasets, they overall support our results that brain network maturation from late childhood until early adulthood implicates micro- and macroscale factors in both subcortical and cortical networks. Coupled network and molecular changes may ultimately change subcortical and cortical circuit properties, including the balance of excitation and inhibition (E/I). Human brain development involves spatio-temporal waves of gene expression changes across different brain regions and developmental time windows (Ip et al., 2010; Kang et al., 2011; Shin et al., 2018). In the study of adolescent development, prior studies have suggested shifts in E/I balance, evolving from a dominant inhibitory bias in early developmental stages towards stronger excitatory drive in later stages, and suggested that these may underlie the maturation of cognitive functions such as working memory and executive control (Dorrn et al., 2010; Lander et al., 2017; Liu et al., 2007). In common neurodevelopmental disorders, including autism, schizophrenia, and attention deficit hyperactivity disorder, imbalances in cortical E/I and cortico-subcortical network function have been demonstrated (Cellot and Cherubini, 2014; Gandal et al., 2018; Lee et al., 2017; Lewis et al., 2005; Nelson and Valakh, 2015; Park et al., 2020a; Sohal and Rubenstein, 2019; Trakoshis et al., 2020), potentially downstream to perturbations of different neurotransmitter systems, such as interneuron-mediated GABA transmission (Bonaventura et al., 2017; Kilb, 2012; Liu et al., 2007; Park et al., 2020a; Silveri et al., 2013; Trakoshis et al., 2020; Tziortzi et al., 2014).

Higher order cognitive function implicates functionally relevant whole-brain network mechanisms, and its prediction may thus leverage structurally governed principles of network integration and segregation. Application of a supervised machine learning framework with cross-validation and regularization to our cohort demonstrated that it is possible to predict inter-individual variations in future IQ from structural connectome manifold data. These findings complement conceptual accounts linking brain organization to cognitive function (Margulies et al., 2016; Mesulam, 1998), and earlier efforts to predict IQ measures from inter-regional measures of connectivity and graph-theoretical indices of network topology (Greene et al., 2018). Notably, evaluations of several feature combinations highlighted that predictive performance was highest when including both baseline and trajectory data, and when complementing cortical and subcortical manifold features. These findings re-emphasize the benefits of incorporating subcortical nodes in the characterization of large-scale cortical network organization and overall cognitive function (Alves et al., 2019; Müller et al., 2020; Shine, 2021; Shine et al., 2019). Of note, although our model significantly outperformed a baseline model, the relationship between the actual and predicted IQ scores did not locate on the equality line and the strength of the association was rather weak. Further improvements in brain-based IQ prediction in adolescence, for example through combinations of structural and functional imaging features, will be a focus of future work.

Adolescence is a time characterized by ongoing brain changes (Baum et al., 2020; Gogtay et al., 2004; Larsen and Luna, 2018; Menon, 2013; Shaw et al., 2006), gradually increasing independence from caregivers, accompanied by strong increments in knowledge and our ability to think more abstractly and to cooperate with our peers to achieve common goals. On the other hand, adolescence is also a sensitive time window for risk taking, the development of addictions, and is associated with high rates of onset of several psychiatric disorders (Hong et al., 2019; Khundrakpam et al., 2017). Our study has shown that structural brain network organization continues to mature significantly during this time period, with higher order association cortices in prefrontal and posterior regions especially showing an expansion of their corresponding connectome manifold signature. Findings were related to an increased strengthening of intra-community connectivity as well as cortico-subcortical connectivity to thalamo-striatal regions. Although the current work was restricted to a longitudinal sample of typically developing adolescents, our framework may be useful to explore multi-scale network perturbations in cohorts with a psychiatric diagnosis or those at risk for addiction or atypical neurodevelopment.

METHODS

Participants

We obtained imaging and phenotypic data from the NSPN 2400 cohort, which contains questionnaire data on 2,402 individuals (with MRI data on a subset of ~300) from adolescence to young adulthood in a longitudinal setting (Kiddle et al., 2018; Whitaker et al., 2016). The NSPN study was ethically approved by the National Research Ethics Service and conducted in accordance with NHS research governance standards. All participants provided informed consent in writing, with additional parental consent for participants aged less than 16 years at enrolment. Included participants completed quality-controlled (see *Data preprocessing* section) multimodal MRI scans consisting of T1-weighted, MT, and dMRI for at least two time points. Our final sample consisted of a total of 208 participants (48% female; mean (range) age = 18.82 (14–25) years at baseline and 19.95 (15–26) at follow-up; inter-scan interval of 11.28 (6–12) months), collected from three different UK sites: Wolfson Brain Imaging Centre and MRC Cognition and Brain Sciences Unit in Cambridge; and University College London. We divided the participants into template and non-template cohorts with matched age, sex, and site ratio. The template dataset (n = 30; 50% female; mean (range) age = 18.69 (15–24) years at baseline and 19.84 ± 2.66 (16–25) at follow-up) was used for constructing the group mean template manifold and the non-template dataset (n = 178; 47% female; mean (range) age = 18.84 (14–25) years at baseline and 19.97 (15–26) at follow-up) was used for conducting main analyses. Of note, changing the template dataset composition did not markedly affect main findings (**Fig. S16**).

MRI acquisition

Imaging data were obtained using Siemens Magnetom TIM Trio 3T scanners. T1-weighted and MT sequences were acquired using a quantitative multiparameter mapping (MPM) sequence (repetition time (TR)/flip angle = 18.7ms/20º for T1-weighted and 23.7ms/6º for MT; six equidistance echo times (TE) = 2.2–14.7ms; voxel size = 1mm^3; 176 slices; field of view (FOV) = 256 × 240mm; matrix size = 256 × 240 × 176) (Weiskopf et al., 2013). The dMRI data were acquired using a spin-echo echo-planar imaging (EPI) sequence (TR = 8,700ms; TE = 90ms; flip angle = 90º; voxel size = 2mm^3; 70 slices; FOV = 192 × 192mm^2; matrix size = 96 × 96 × 70; b-value = 1,000s/mm^2; 63 diffusion

directions; and 6 b0 images).

Data preprocessing

T1-weighted data were processed using the fusion of neuroimaging preprocessing (FuNP) pipeline integrating AFNI, FSL, FreeSurfer, ANTs, and Workbench (Avants et al., 2011; Cox, 1996; Fischl, 2012; Glasser et al., 2013; Jenkinson et al., 2012; Park et al., 2019), which is similar to the minimal preprocessing pipeline for the Human Connectome Project (Glasser et al., 2013). Gradient nonlinearity and b0 distortion correction, non-brain tissue removal, and intensity normalization were performed. The white matter and pial surfaces were generated by following the boundaries between different tissues (Dale et al., 1999), and they were averaged to generate the midthickness contour, which was used to generate the inflated surface. The spherical surface was registered to the Conte69 template with 164k vertices (Van Essen et al., 2012) and downsampled to a 32k vertex mesh. Quality control involved visual inspection of surface reconstruction of T1-weighted data, and cases with faulty cortical segmentation were excluded. Surface-based co-registration between T1-weighted and MT weighted scans were performed. We generated 14 equivolumetric cortical surfaces within the cortex and sampled MT intensity along these surfaces (Paquola et al., 2019a). The vertex-wise MT profiles for each surface depth were averaged based on the Schaefer atlas with 200 parcels (Schaefer et al., 2018). The dMRI data were processed using MRtrix3 (Tournier et al., 2019), including correction for susceptibility distortions, head motion, and eddy currents. We visually inspected the quality of co-registration between the adolescence data and adult-driven surface template as well as parcellation atlas, and all data showed reasonable registration results.

Structural connectome manifold identification

Structural connectomes were generated from preprocessed dMRI data (Tournier et al., 2019). Anatomically constrained tractography was performed using different tissue types derived from the T1-weighted image, including cortical and subcortical grey matter, white matter, and cerebrospinal fluid (Smith et al., 2012). Multi-shell and multi-tissue response functions were estimated (Christiaens et al., 2015), and constrained spherical-deconvolution and intensity normalization were performed (Jeurissen et al., 2014). The tractogram was generated with 40 million streamlines, with a maximum tract length of 250 and a fractional anisotropy cutoff of 0.06. Subsequently, spherical-deconvolution informed filtering of tractograms (SIFT2) was applied to reconstruct whole-brain streamlines weighted by the cross-section multipliers, which considers the fiber bundle's total intra-axonal space across its full cross-sectional extent (Smith et al., 2015). The structural connectome was built by mapping the reconstructed cross-section streamlines onto the Schaefer 7-network based atlas with 200 parcels (Schaefer et al., 2018) then log-transformed to adjust for the scale (Fornito et al., 2016). We opted for this atlas as it (i) allows contextualization of our findings within macroscale intrinsic functional communities (Yeo et al., 2011), (ii) incorporates the option to assess results across different granularities, and (iii) aligns the current study with previous work from our group (Benkarim et al., 2020; Paquola et al., 2020; Park et al., 2021, 2020a; Rodríguez-Cruces et al., 2020) and others (Baum et al., 2020; Betzel et al., 2019; Osmanlıoğlu et al., 2019).

Cortex-wide structural connectome manifolds were identified using BrainSpace (https://github.com/MICA-MNI/BrainSpace) (Vos de Wael et al., 2020). First, a template manifold was estimated using a group representative structural connectome of the template dataset. The group

representative structural connectome was defined using a distance-dependent thresholding that preserves long-range connections (Betzel et al., 2019). An affinity matrix was constructed with a normalized angle kernel, and eigenvectors were estimated via diffusion map embedding (**Fig. 1A**), a non-linear dimensionality reduction technique (Coifman and Lafon, 2006) that projects connectome features into low dimensional manifolds (Margulies et al., 2016). This technique is only controlled by few parameters, computationally efficient, and relatively robust to noise compared to other non-linear techniques (Errity and McKenna, 2007; Gallos et al., 2020; Hong et al., 2020; Tenenbaum et al., 2000), and has been extensively used in the previous gradient mapping literature (Hong et al., 2019, 2020; Huntenburg et al., 2017; Larivière et al., 2020a; Margulies et al., 2016; Müller et al., 2020; Paquola et al., 2019a; Park et al., 2021; Sofie L. Valk et al., 2020; Vos de Wael et al., 2020). It is controlled by two parameters α and *t*, where α controls the influence of the density of sampling points on the manifold (α = 0, maximal influence; α = 1, no influence) and *t* controls the scale of eigenvalues of the diffusion operator. We set α = 0.5 and t = 0 to retain the global relations between data points in the embedded space, following prior applications (Hong et al., 2019; Margulies et al., 2016; Paquola et al., 2019a, 2019b; Vos de Wael et al., 2020). Briefly, the eigenvectors estimated from the decomposition technique generate a connectivity coordinate system (Bijsterbosch et al., 2020; Haak et al., 2018; Huntenburg et al., 2018; Margulies et al., 2016; Mars et al., 2018) – the diffusion map, where Euclidian distances in the manifold correspond to diffusion times between the nodes of the network (Coifman and Lafon, 2006). In this manifold space, interconnected brain regions with similar connectivity patterns are closely located, and regions with weak similarity in connectivity patterns are located farther apart. After generating the template manifold, individual-level manifolds were estimated from the non-template dataset and aligned to the template manifold via Procrustes alignment (Langs et al., 2015; Vos de Wael et al., 2020). To analyze change in the low dimensional manifold space, we simplified the multivariate eigenvectors into a single scalar value *i.e.,* manifold eccentricity (**Fig. 1B**). Manifold eccentricity was calculated as the Euclidean distance between the manifold origin and all data points (*i.e.,* brain regions) in manifold space. The template center was defined as the centroid of the first three eigenvectors, which explained 50% variance. Specifically, manifold eccentricity was defined as follows:

$$C_T = \frac{1}{N}\left[\sum_{i=1}^{N} T(E1)_i, \sum_{i=1}^{N} T(E2)_i, \sum_{i=1}^{N} T(E3)_i\right] \quad (1)$$

$$ME = \sqrt{\sum_{e=1}^{3}\{I(E_e) - C_T(e)\}^2} \quad (2)$$

C_T is the template manifold origin; N number of brain regions; $T(\cdot)$ template manifold; ME manifold eccentricity; $I(\cdot)$ individual manifold; $C_T(e)$ origin of eth template manifold. Simply, as shown in **Fig. S17**, each brain region (*i.e.,* each dot in the scatter plot) is described as a vector from the manifold origin (*i.e.,* triangular mark in the scatter plot), and manifold eccentricity is simply a length (*i.e.,* Euclidean distance) of that vector. Shifts in connectivity patterns of a given region thus will lead to shifts in the vectors, which in turn changes the manifold eccentricity. Thus, manifold eccentricity quantifies global brain organization based in the connectivity space.

Age-related changes in structural manifolds

We assessed changes in manifold eccentricity across age using a linear mixed effect model (Worsley et al., 2009), controlling for effects of sex, site, head motion, and subject-specific random intercept to improve model fit in accelerated longitudinal designs. The t-statistics of each brain region were

computed and we corrected for multiple comparisons by using a FDR threshold of $q < 0.05$ (**Fig. 1C**) (Benjamini and Hochberg, 1995). We stratified age-related effects based on a seminal model of neural organization and laminar differentiation that contains four cortical hierarchical levels (Mesulam, 1998), as well as seven intrinsic functional communities (Yeo et al., 2011) (**Fig. 1D**). To assess the effects with respect to age^2, we repeated implementing a linear mixed effect model by adding a quadratic term of age to the model.

To provide the underlying structure of manifold eccentricity, we compared the changes in manifold eccentricity with those in connectome topology measures. We first defined clusters within the identified regions based on their spatial boundaries (**Fig. S1A**). Then, we calculated degree centrality, as well as modular measures of within-module degree and participation coefficient using the Brain Connectivity Toolbox (https://sites.google.com/site/bctnet/) (Rubinov and Sporns, 2010) and connectivity distance using a recently published approach (Larivière et al., 2020b). Degree centrality is defined as the row-wise sum of the weighted connectivity matrix, representing the connection strength of a given node (Rubinov and Sporns, 2010). Connectivity distance is a given brain region's geodesic distance to its structurally connected brain areas within the cortex (Oligschläger et al., 2019), and it is defined as the multiplication between the geodesic distance and the binarized structural connectome (Hong et al., 2019; Oligschläger et al., 2019). Within-module degree and participation coefficient are nodal measures reflecting different facets of community organization (Rubinov and Sporns, 2010). For each individual subject, community structure was defined using Louvain's algorithm (Blondel et al., 2008) and a consistency matrix was constructed, where each element of the matrix represents whether the two different nodes are involved in the same community (*i.e.,* 1) or not (*i.e.,* 0) (**Fig. S2A**). We constructed the group-wise consistency matrix by averaging the consistency matrix of all subjects and applied k-means clustering (**Fig. S2B**). The optimal number of clusters was determined using the silhouette coefficient, *i.e.,* the k that maximized the silhouette coefficient (Kannan et al., 2010). We calculated within-module degree and participation coefficient based on these modules. Within-module degree is the degree centrality within a community, indicating intra-community connection strength, while participation coefficient represents inter-community connectivity (Rubinov and Sporns, 2010). We calculated linear correlations between changes in manifold eccentricity and those in each graph-theoretical measure for each cluster (**Fig. S1B**). The significance of the correlation was corrected using 1,000 permutation tests by randomly shuffling subject indices in one of the data vectors, and we corrected for multiple comparisons across clusters using an FDR procedure (Benjamini and Hochberg, 1995). To visualize age-related changes in these parameters, we stratified each measure according to discretized age bins (< 17, 17-19, 19-21, 21-23, ≥ 23; **Fig. S3**).

Cortical morphology and microstructure

It has been shown that macroscale cortical morphology and microstructure significantly change during development (Gogtay et al., 2004; Khundrakpam et al., 2017; Paquola et al., 2019a; Shaw et al., 2006). Here, we confirmed these changes by assessing age-related changes in MRI-based cortical thickness measures and intracortical measures of MT, an index sensitive to myelin content (Weiskopf et al., 2013), using linear mixed effect models (**Fig. 2A**) (Worsley et al., 2009). We further regressed out cortical thickness and MT from the connectome manifold eccentricity metric. We then implemented linear mixed effect models using the residuals of manifold measures to assess whether

age-related connectome manifold effects exist above and beyond age-related effects on cortical morphology and microstructure (**Fig. 2B**).

Subcortico-cortical connectivity

To assess age-related changes in subcortical manifold organizations in addition to cortical manifold structures, we first parcellated the accumbens, amygdala, caudate, hippocampus, pallidum, putamen, and thalamus for each individual (Patenaude et al., 2011), and approximated cross-section streamlines connect each subcortical region to the rest of the brain. For each individual and each subcortical region, we projected the streamline strength to cortical manifold space by weighting the cortical manifolds with the streamline strength of the connection between each subcortical region and cortical parcels, yielding a matrix with the form of (number of brain regions × number of cortical manifolds). We averaged the matrix across the axis of cortical manifolds to construct subcortical-weighted manifold vector. We assessed age-related changes in the subcortical-weighted manifold using a linear mixed effect model (Worsley et al., 2009), controlling for sex, site, head motion, and subject-specific random intercept, and FDR corrected for multiple comparisons (**Fig. 3**) (Benjamini and Hochberg, 1995).

Transcriptomic analysis

We performed spatial correlation analysis to *post-mortem* gene expression data and carried out a developmental enrichment analysis (**Fig. 4**). In brief, we first correlated the t-statistics map, which represents age-related changes in manifold eccentricity that controlled for cortical morphology and microstructure, with the *post-mortem* gene expression maps provided by the Allen Institute using the Neurovault gene decoding tool (Gorgolewski et al., 2015, 2014; Hawrylycz et al., 2012). Leveraging mixed effect models to associate the input t-statistic map with the genes of six donor brains, Neurovault yields the gene symbols associated with the input spatial map. Gene symbols that passed for a significance level of FDR < 0.05 were further tested whether they are consistently expressed across different donors using abagen toolbox (https://github.com/rmarkello/abagen) (Arnatkeviciute et al., 2019; Hawrylycz et al., 2012; Markello et al., 2020). For each gene, we estimated whole-brain gene expression map and correlated it between all pairs of donors. Leveraging cell-type specific expression analysis (CSEA) developmental expression tool (http://genetics.wustl.edu/jdlab/csea-tool-2) (Dougherty et al., 2010; Xu et al., 2014), we evaluated the significance of overlap between the genes showing consistent whole-brain expression pattern across donors (FDR < 0.05) with RNAseq data obtained from BrainSpan dataset (http://www.brainspan.org). The significance was calculated based on Fisher's exact test (Fisher, 1922) with FDR correction (Benjamini and Hochberg, 1995). The CSEA tool provides simplified results of gene enrichment profiles along six major brain regions (*i.e.,* cortex, thalamus, striatum, cerebellum, hippocampus, amygdala) across ten developmental periods (from early fetal to young adulthood) approximated from mouse data, yielding a total of 60 combinations of developmental enrichment profiles (Xu et al., 2014). We repeated developmental enrichment analysis using the genes identified from the rotated maps of the age-related changes in manifold eccentricity (100 spherical rotations). For each iteration, we obtained developmental expression profiles using the identified genes, where the FDR-corrected p-values built a null distribution. For each brain division and developmental period, if the actual p-value placed outside 95% of the null distribution, it was deemed significant. As the Allen Brain Institute repository

is composed of adult *post-mortem* datasets, it should be noted that the associated gene symbols represent indirect associations with the input t-statistic map derived from the developmental data.

Association with the development of cognitive function

Leveraging a supervised machine learning with ten-fold cross-validation, we predicted full IQ score measured by Wechsler Abbreviated Scale of Intelligence (Wechsler, 1999) at follow-up using cortical and subcortical features. Four different feature sets were evaluated: (1) manifold eccentricity of the identified cortical regions at baseline and (2) manifold eccentricity at baseline and its longitudinal change (*i.e.,* differences between follow-up and baseline), and (3) cortical manifold eccentricity and subcortical-weighted manifold of the identified regions at baseline and (4) manifold eccentricity and subcortical-weighted manifold at baseline and their longitudinal changes. For each evaluation, a subset of features that could predict future IQ was identified using elastic net regularization ($\rho = 0.5$) with optimized regularization parameters (L1 and L2 penalty terms) via nested ten-fold cross-validation (Cawley and Talbot, 2010; Parvandeh et al., 2020; Tenenbaum et al., 2000; Varma and Simon, 2006; Zou and Hastie, 2005). We split the dataset into training (9/10) and test (1/10) partitions, and each training partition was further split into inner training and testing folds using another ten-fold cross-validation. Within the inner fold, elastic net regularization finds a set of non-redundant features to explain the dependent variable. Using a linear regression, we predicted the IQ scores of inner fold test data using the features of the selected brain regions by controlling for age, sex, site, and head motion. The model with minimum mean absolute error (MAE) across the inner folds was applied to the test partition of the outer fold, and the IQ scores of outer fold test data were predicted. The prediction procedure was repeated 100 times with different training and test sets to reduce subject selection bias. Prediction accuracy was indexed by computing linear correlations between the actual and predicted IQ scores as well as MAE. A 95% confidence interval of the accuracy measures was also reported. Permutation-based correlations across 1,000 tests were conducted by randomly shuffling subject indices to check whether the prediction performance exceeded chance levels. To assess whether our model outperforms baseline model, we predicted IQ of test data using average of IQ of training data (*i.e.,* predicted IQ = mean(training set IQ)). The improvement of prediction performance was assessed using Meng's z-test (Meng et al., 1992). In addition to predicting future IQ, we performed the same prediction analysis to predict the change of IQ between the baseline and follow-up.

Sensitivity analysis

a) Spatial scale. To assess the consistency of our findings across spatial scales, we additionally performed the linear mixed effect modeling using a finer parcellation scheme of 300 parcels (**Fig. S5**) (Schaefer et al., 2018).

b) Site and sex effect. Participants were recruited from three different sites. To assess whether the longitudinal changes in manifold eccentricity across age are consistent across different sites, we calculated interaction effects of the relationship between age and manifold eccentricity of the identified regions across sites (**Fig. S6B**). In addition, we computed interaction effect of the relationship between age and manifold eccentricity across male and female subjects to assess whether the age-related changes are affected by biological sexes (**Fig. S6C**).

c) Different parameters for diffusion map embedding. To assess the sensitivity of our findings, we generated connectome manifolds with different parameters for diffusion map embedding (α = 0.25, 0.5, 0.75; t = 0, 1, 2, 3). We assessed age-related changes of the newly defined manifold eccentricity and calculated linear correlation with t-statistic map of the default setting (α = 0.5; t = 0; *Fig. 1C*).

d) Gradient alignment fidelity. To assess robustness of individual alignment, we computed linear correlations between the template and individual manifolds before and after alignment. We also repeated the linear mixed effect modeling after excluding 10% of subjects with the lowest alignment to the template manifold.

e) Connectome manifold generation using principal component analysis. To explore consistency of our results when using different dimensionality reduction techniques, we generated connectome manifolds using principal component analysis (Wold et al., 1987), instead of relying on diffusion map embedding (Coifman and Lafon, 2006), and performed longitudinal modeling (**Fig. S8**). We compared the eigenvectors estimated from diffusion map embedding and principal component analysis using linear correlations.

f) Longitudinal changes in graph-theoretical measures. To compare longitudinal changes in manifold eccentricity with those in graph-theoretical centrality measures, we calculated betweenness, degree, and eigenvector centrality of the structural connectomes and build similar linear mixed effects models to assess longitudinal change (**Fig. S9**). Betweenness centrality is the number of weighted shortest paths between any combinations of nodes that run through that node, degree centrality is the sum of edge weights connected to a given node, and eigenvector centrality measures the influence of a node in the whole network (Lohmann et al., 2010; Rubinov and Sporns, 2010; Zuo et al., 2012). Spatial similarity between t-statistics of centrality and manifold measures were assessed with 1,000 spin tests that account for spatial autocorrelation (Alexander-Bloch et al., 2018).

g) Manifold eccentricity analysis based on all eigenvectors. We repeated our analysis by calculating manifold eccentricity from all eigenvectors to assess consistency of the findings (**Fig. S10**).

h) Robustness of group representative structural connectome. We compared the distance-dependent thresholding (Betzel et al., 2019) that was adopted for the main analysis with a consistency thresholding approach (Wang et al., 2019). The latter averages subject specific matrices, in addition to performing a 50, 40, 30, 20, 10% thresholding, as well as simple averaging (*i.e.,* 0% thresholding) (**Fig. S11**).

i) Connectome manifolds based on structural parcellation. To confirm whether functional and structural parcellation schemes yield consistent results, we repeated our main analyses using 200 cortical nodes structural parcellation scheme, which preserves the macroscopic boundaries of the Desikan-Killiany atlas (Desikan et al., 2006; Vos de Wael et al., 2020) (**Fig. S12**).

j) Longitudinal modeling using edge weights. In addition to the analyses based on manifold eccentricity, linear mixed effect modeling using connectome edge weights assessed age-related longitudinal changes in streamline strength (**Fig. S13**).

k) Manifold eccentricity and pubertal stages. To assess the relationship between manifold eccentricity and pubertal stages, we selected a subset of participants who completed Tanner scale (Marshall and Tanner, 1970, 1969), which quantifies pubertal stages from 1 (pre-puberty) to 5 (final phase of physical maturation). However, the score was collected at baseline and for 73/208 participants only. To confirm robustness, we performed linear mixed effect modeling using this subset (**Fig. S14A**). In

addition, we assessed interaction effects of Tanner scale and manifold eccentricity restricted to the regions identified from the overall sample (**Fig. S14B**).

l) IQ prediction using non-linear model. We additionally performed prediction analysis for predicting future IQ score using regression tree method (*i.e.,* decision tree learning), a non-linear approach based on tree model constituting root node and split leaf nodes, where the leaf nodes contain the response variables (Breiman et al., 1984) (**Fig. S15**).

DATA AND CODE AVAILABILITY

The imaging and phenotypic data were provided by the Neuroscience in Psychiatry Network (NSPN) 2400 cohort. As stated in https://doi.org/10.1093/ije/dyx117, the NSPN project is committed to make the anonymised dataset fully available to the research community, and participants have consented to their de-identified data being made available to other researchers. A data request can be made to openNSPN@medschl.cam.ac.uk. Codes for connectome manifold generation are available at https://github.com/MICA-MNI/BrainSpace and those for calculating manifold eccentricity and subcortical-weighted manifold, as well as performing linear mixed effect modeling to assess age-effects on these features at https://github.com/MICA-MNI/micaopen/tree/master/manifold_features.

ACKNOWLEDGEMENTS

Dr. Bo-yong Park was funded by the National Research Foundation of Korea (NRF-2020R1A6A3A03037088), Molson Neuro-Engineering fellowship by Montreal Neurological Institute and Hospital (MNI), and a postdoctoral fellowship of the Fonds de la Recherche du Quebec – Santé (FRQ-S). Dr. Richard A. I. Bethlehem was funded by a British Academy Post-Doctoral Fellowship and the Autism Research Trust. Dr. Casey Paquola and Dr Raul R. Cruces were funded through postdoctoral fellowships of the FRQ-S. Ms. Sara Larivière acknowledges funding from the Canadian Institutes of Health Research (CIHR). Dr. Edward T. Bullmore was supported by a Senior Investigator award from the National Institute of Health Research (NIHR). Dr. Boris C. Bernhardt acknowledges research support from the National Science and Engineering Research Council of Canada (NSERC Discovery-1304413), the CIHR (FDN-154298), SickKids Foundation (NI17-039), Azrieli Center for Autism Research (ACAR-TACC), BrainCanada, FRQ-S, and the Tier-2 Canada Research Chairs program. Drs. Bo-yong Park, Richard A. I. Bethlehem, Casey Paquola, and Boris C. Bernhardt are jointly funded through an MNI-Cambridge collaborative award. The Neuroscience and Psychiatry Network (NSPN) study was funded by a Wellcome Trust award to the University of Cambridge and University College London. The data were curated and analyzed using a computational facility funded by an MRC research infra-structure award (MR/M009041/1) and supported by the NIHR Cambridge Biomedical Research Centre. The views expressed are those of the authors and not necessarily those of the NHS, the NIHR or the Department of Health and Social Care.

AUTHOR CONTRIBUTIONS

B.P. and B.C.B. designed the experiments, analyzed the data, and wrote the manuscript. R.A.I.B. aided data curation. R.A.I.B., C.P., S.L., R.R.C., and R.V.D.W. aided with the experiments. E.T.B. designed the NSPN MRI study and edited the manuscript. B.P. and B.C.B. are the corresponding authors of this work and have responsibility for the integrity of the data analysis.

CONFLICT OF INTEREST

E.T.B. serves on the scientific advisory board of Sosei Heptares and as a consultant for GlaxoSmithKline. The other authors declare no conflicts of interest.

REFERENCES

Aglioti S. 1997. The role of the thalamus and basal ganglia in human cognition. *J Neurolinguistics* **10**:255–265. doi:10.1016/S0911-6044(97)00020-1

Alexander-Bloch AF, Shou H, Liu S, Satterthwaite TD, Glahn DC, Shinohara RT, Vandekar SN, Raznahan A. 2018. On testing for spatial correspondence between maps of human brain structure and function. *Neuroimage* **178**:540–551. doi:10.1016/j.neuroimage.2018.05.070

Alexander GE, Crutcher MD. 1990. Functional architecture of basal ganglia circuits: neural substrates of parallel processing. *Trends Neurosci* **13**:266–271. doi:10.1016/0166-2236(90)90107-L

Altmann A, Ryten M, Nunzio M Di, Ravizza T, Tolomeo D, Reynolds RH, Somani A, Bacigaluppi M, Iori V, Micotti E, Botia JA, Absil J, Alhusaini S, Alvim MKM, Auvinen P, Bargallo N, Bartolini E, Bender B, Bergo F, Bernardes T, Bernasconi A, Bernasconi N, Bernhardt BC, Blackmon K, Braga B, Caligiuri ME, Cavalo A, Carlson C, Carr S, Cavalleri G, Cendes F, Chen J, Chen S, Cherubini A, Concha L, David P, Delanty N, Depondt C, Devinsky O, Doherty CP, Domin M, Focke N, Foley S, Franca W, Gambardella A, Guerrini R, Hamandi K, Hibar DP, Isaev DY, Jackson G, Jahanshad N, Kalviainen R, Keller S, Kochunov P, Kotikalapudi R, Kowalczyk MA, Kuzniecky R, Kwan P, Labate A, Langer S, Lenge M, Liu M, Martin P, Mascalchi M, Meletti S, Morita ME, O'Brien TJ, Pariente JC, Richardson MP, Rodriguez-Cruces R, Rummel C, Saavalainen T, Semmelroch MK, Severino M, Striano P, Thesen T, Thomas RH, Tondelli M, Tortora D, Vaudano AE, Vivash L, Podewils F von, Wagner J, Weber B, Wiest R, Yasuda CL, Zhang G, Zhang J, Group E-EW, Leu C, Avbersek A, Consortium E, Thom M, Whelan CD, Thompson P, McDonald C, Vezzani A, Sisodiya SM. 2018. A systems-level analysis highlights microglial activation as a modifying factor in common forms of human epilepsy. *bioRxiv* 470518. doi:10.1101/470518

Alves PN, Foulon C, Karolis V, Bzdok D, Margulies DS, Volle E, Thiebaut de Schotten M. 2019. An improved neuroanatomical model of the default-mode network reconciles previous neuroimaging and neuropathological findings. *Commun Biol* **2**:370. doi:10.1038/s42003-019-0611-3

Arnatkeviciute A, Fulcher BD, Fornito A. 2019. A practical guide to linking brain-wide gene expression and neuroimaging data. *Neuroimage* **189**:353–367. doi:10.1016/j.neuroimage.2019.01.011

Ashburner M, Ball CA, Blake JA, Botstein D, Butler H, Cherry JM, Davis AP, Dolinski K, Dwight SS, Eppig JT, Harris MA, Hill DP, Issel-Tarver L, Kasarskis A, Lewis S, Matese JC, Richardson JE, Ringwald M, Rubin GM, Sherlock G. 2000. Gene Ontology: tool for the unification of biology. *Nat Genet* **25**:25–29. doi:10.1038/75556

Avants BB, Tustison NJ, Song G, Cook PA, Klein A, Gee JC. 2011. A reproducible evaluation of ANTs similarity metric performance in brain image registration. *Neuroimage* **54**:2033–2044. doi:10.1016/j.neuroimage.2010.09.025

Baker STE, Lubman DI, Yücel M, Allen NB, Whittle S, Fulcher BD, Zalesky A, Fornito A. 2015. Developmental changes in brain network hub connectivity in late adolescence. *J Neurosci* **35**:9078–9087. doi:10.1523/JNEUROSCI.5043-14.2015

Ball G, Seidlitz J, O'Muircheartaigh J, Dimitrova R, Fenchel D, Makropoulos A, Christiaens D, Schuh A, Passerat-Palmbach J, Hutter J, Cordero-Grande L, Hughes E, Price A, Hajnal J V., Rueckert D, Robinson EC, Edwards AD. 2020. Cortical morphology at birth reflects spatiotemporal patterns of gene expression in the fetal human brain, PLoS Biology.

doi:10.1371/journal.pbio.3000976

Baum GL, Cui Z, Roalf DR, Ciric R, Betzel RF, Larsen B, Cieslak M, Cook PA, Xia CH, Moore TM, Ruparel K, Oathes DJ, Alexander-Bloch AF, Shinohara RT, Raznahan A, Gur RE, Gur RC, Bassett DS, Satterthwaite TD. 2020. Development of structure–function coupling in human brain networks during youth. *Proc Natl Acad Sci U S A* **117**:771–778. doi:10.1073/pnas.1912034117

Benjamini Y, Hochberg Y. 1995. Controlling the False Discovery Rate : A Practical and Powerful Approach to Multiple Testing. *J R Stat Soc* **57**:289–300.

Benkarim O, Paquola C, Park B, Hong S-J, Royer J, Wael RV de, Lariviere S, Valk S, Bzdok D, Mottron L, Bernhardt B. 2020. Functional idiosyncrasy has a shared topography with group-level connectivity alterations in autism. *bioRxiv*. doi:10.1101/2020.12.18.423291

Bethlehem RAI, Paquola C, Seidlitz J, Ronan L, Bernhardt B, Consortium CCAN, Tsvetanov KA. 2020. Dispersion of functional gradients across the adult lifespan. *Neuroimage* **222**:117299. doi:10.1016/j.neuroimage.2020.117299

Betzel RF, Griffa A, Hagmann P, Miši´c B. 2019. Distance-dependent consensus thresholds for generating group-representative structural brain networks. *Netw Neurosci* **3**:475–496. doi:10.1162/netn_a_00075

Bijsterbosch J, Harrison SJ, Jbabdi S, Woolrich M, Beckmann C, Smith S, Duff EP. 2020. Challenges and future directions for representations of functional brain organization. *Nat Neurosci* **23**:1484–1495. doi:10.1038/s41593-020-00726-z

Blazquez Freches G, Haak K V., Bryant KL, Schurz M, Beckmann CF, Mars RB. 2020. Principles of temporal association cortex organisation as revealed by connectivity gradients. *Brain Struct Funct* **225**:1245–1260. doi:10.1007/s00429-020-02047-0

Blondel VD, Guillaume JL, Lambiotte R, Lefebvre E. 2008. Fast unfolding of communities in large networks. *J Stat Mech Theory Exp* **2008**. doi:10.1088/1742-5468/2008/10/P10008

Bonaventura J, Quiroz C, Cai NS, Rubinstein M, Tanda G, Ferré S. 2017. Key role of the dopamine D4 receptor in the modulation of corticostriatal glutamatergic neurotransmission. *Sci Adv* **3**:e1601631. doi:10.1126/sciadv.1601631

Breiman L, Friedman J, Stone CJ, Olshen RA. 1984. Classification and Regression Trees. Wadsworth, Inc.

Brown HS, May AE. 1979. A test-retest reliability study of the Wechsler Adult Intelligence Scale. *J Consult Clin Psychol* **47**:601–602. doi:10.1037/0022-006X.47.3.601

Buckner RL, Krienen FM. 2013. The evolution of distributed association networks in the human brain. *Trends Cogn Sci* **17**:648–665. doi:10.1016/j.tics.2013.09.017

Canivez GL, Watkins MW. 1998. Long-term stability of the Wechsler Intelligence Scale for Children--Third Edition. *Psychol Assess* **10**:285–291. doi:10.1037//1040-3590.10.3.285

Carbon S, Douglass E, Dunn N, Good B, Harris NL, Lewis SE, Mungall CJ, Basu S, Chisholm RL, Dodson RJ, Hartline E, Fey P, Thomas PD, Albou LP, Ebert D, Kesling MJ, Mi H, Muruganujan A, Huang X, Poudel S, Mushayahama T, Hu JC, LaBonte SA, Siegele DA, Antonazzo G, Attrill H, Brown NH, Fexova S, Garapati P, Jones TEM, Marygold SJ, Millburn GH, Rey AJ, Trovisco V, Dos Santos G, Emmert DB, Falls K, Zhou P, Goodman JL, Strelets VB, Thurmond J, Courtot M, Osumi DS, Parkinson H, Roncaglia P, Acencio ML, Kuiper M, Lreid A, Logie C, Lovering RC, Huntley RP, Denny P, Campbell NH, Kramarz B, Acquaah V,

Ahmad SH, Chen H, Rawson JH, Chibucos MC, Giglio M, Nadendla S, Tauber R, Duesbury MJ, Del NT, Meldal BHM, Perfetto L, Porras P, Orchard S, Shrivastava A, Xie Z, Chang HY, Finn RD, Mitchell AL, Rawlings ND, Richardson L, Sangrador-Vegas A, Blake JA, Christie KR, Dolan ME, Drabkin HJ, Hill DP, Ni L, Sitnikov D, Harris MA, Oliver SG, Rutherford K, Wood V, Hayles J, Bahler J, Lock A, Bolton ER, De Pons J, Dwinell M, Hayman GT, Laulederkind SJF, Shimoyama M, Tutaj M, Wang SJ, D'Eustachio P, Matthews L, Balhoff JP, Aleksander SA, Binkley G, Dunn BL, Cherry JM, Engel SR, Gondwe F, Karra K, MacPherson KA, Miyasato SR, Nash RS, Ng PC, Sheppard TK, Shrivatsav Vp A, Simison M, Skrzypek MS, Weng S, Wong ED, Feuermann M, Gaudet P, Bakker E, Berardini TZ, Reiser L, Subramaniam S, Huala E, Arighi C, Auchincloss A, Axelsen K, Argoud GP, Bateman A, Bely B, Blatter MC, Boutet E, Breuza L, Bridge A, Britto R, Bye-A-Jee H, Casals-Casas C, Coudert E, Estreicher A, Famiglietti L, Garmiri P, Georghiou G, Gos A, Gruaz-Gumowski N, Hatton-Ellis E, Hinz U, Hulo C, Ignatchenko A, Jungo F, Keller G, Laiho K, Lemercier P, Lieberherr D, Lussi Y, Mac-Dougall A, Magrane M, Martin MJ, Masson P, Natale DA, Hyka NN, Pedruzzi I, Pichler K, Poux S, Rivoire C, Rodriguez-Lopez M, Sawford T, Speretta E, Shypitsyna A, Stutz A, Sundaram S, Tognolli M, Tyagi N, Warner K, Zaru R, Wu C, Chan J, Cho J, Gao S, Grove C, Harrison MC, Howe K, Lee R, Mendel J, Muller HM, Raciti D, Van Auken K, Berriman M, Stein L, Sternberg PW, Howe D, Toro S, Westerfield M. 2019. The Gene Ontology Resource: 20 years and still GOing strong. *Nucleic Acids Res* **47**:D330–D338. doi:10.1093/nar/gky1055

Catron DW. 1978. Immediate Test-Retest Changes in WAIS Scores among College Males. *Psychol Rep* **43**:279–290. doi:10.2466/pr0.1978.43.1.279

Cawley GC, Talbot NLC. 2010. On over-fitting in model selection and subsequent selection bias in performance evaluation. *J Mach Learn Res* **11**:2079–2107.

Cellot G, Cherubini E. 2014. GABAergic signaling as therapeutic target for autism spectrum disorders. *Front Pediatr* **2**:70. doi:10.3389/fped.2014.00070

Chen EY, Tan CM, Kou Y, Duan Q, Wang Z, Meirelles GV, Clark NR, Ma'ayan A. 2013. Enrichr: interactive and collaborative HTML5 gene list enrichment analysis tool. *BMC Bioinformatics* **14**:128. doi:10.1186/1471-2105-14-128

Christiaens D, Reisert M, Dhollander T, Sunaert S, Suetens P, Maes F. 2015. Global tractography of multi-shell diffusion-weighted imaging data using a multi-tissue model. *Neuroimage* **123**:89–101. doi:10.1016/j.neuroimage.2015.08.008

Coifman RR, Lafon S. 2006. Diffusion maps. *Appl Comput Harmon Anal* **21**:5–30. doi:10.1016/j.acha.2006.04.006

Cox RW. 1996. AFNI : Software for Analysis and Visualization of Functional Magnetic Resonance Neuroimages. *Comput Biomed Res* **29**:162–173. doi:10.1006/cbmr.1996.0014

Crespi BJ. 2016. Autism as a disorder of high intelligence. *Front Neurosci* **10**:300. doi:10.3389/fnins.2016.00300

Dale AM, Fischl B, Sereno MI. 1999. Cortical surface-based analysis: I. Segmentation and surface reconstruction. *Neuroimage* **9**:179–194. doi:10.1006/nimg.1998.0395

Desikan RS, Ségonne F, Fischl B, Quinn BT, Dickerson BC, Blacker D, Buckner RL, Dale AM, Maguire RP, Hyman BT, Albert MS, Killiany RJ. 2006. An automated labeling system for subdividing the human cerebral cortex on MRI scans into gyral based regions of interest. *Neuroimage* **31**:968–980. doi:10.1016/j.neuroimage.2006.01.021

Dorrn AL, Yuan K, Barker AJ, Schreiner CE, Froemke RC. 2010. Developmental sensory

experience balances cortical excitation and inhibition. *Nature* **465**:932–936. doi:10.1038/nature09119

Dougherty JD, Schmidt EF, Nakajima M, Heintz N. 2010. Analytical approaches to RNA profiling data for the identification of genes enriched in specific cells. *Nucleic Acids Res* **38**:4218–4230. doi:10.1093/nar/gkq130

Errity A, McKenna J. 2007. A Comparative Study of Linear and Nonlinear Dimensionality Reduction for Speaker Identification2007 15th International Conference on Digital Signal Processing. IEEE. pp. 587–590. doi:10.1109/ICDSP.2007.4288650

Fischl B. 2012. FreeSurfer. *Neuroimage* **62**:774–781. doi:10.1016/j.neuroimage.2012.01.021

Fisher RA. 1922. On the Interpretation of χ 2 from Contingency Tables, and the Calculation of P. *J R Stat Soc* **85**:87. doi:10.2307/2340521

Fornito A, Arnatkevičiūtė A, Fulcher BD. 2019. Bridging the Gap between Connectome and Transcriptome. *Trends Cogn Sci* **23**:34–50. doi:10.1016/j.tics.2018.10.005

Fornito A, Zalesky A, Bullmore E. 2016. Fundamentals of Brain Network Analysis. Amsterdam: Academic Press.

Gallos IK, Galaris E, Siettos CI. 2020. Construction of embedded fMRI resting-state functional connectivity networks using manifold learning. *Cogn Neurodyn* **0123456789**. doi:10.1007/s11571-020-09645-y

Gandal MJ, Zhang P, Hadjimichael E, Walker RL, Chen C, Liu S, Won H, Van Bakel H, Varghese M, Wang Y, Shieh AW, Haney J, Parhami S, Belmont J, Kim M, Losada PM, Khan Z, Mleczko J, Xia Y, Dai R, Wang D, Yang YT, Xu M, Fish K, Hof PR, Warrell J, Fitzgerald D, White K, Jaffe AE, Peters MA, Gerstein M, Liu C, Iakoucheva LM, Pinto D, Geschwind DH. 2018. Transcriptome-wide isoform-level dysregulation in ASD, schizophrenia, and bipolar disorder. *Science (80-)* **362**:1265. doi:10.1126/science.aat8127

Garde E, Lykke Mortensen E, Rostrup E, Paulson OB. 2005. Decline in intelligence is associated with progression in white matter hyperintensity volume. *J Neurol Neurosurg Psychiatry* **76**:1289–1291. doi:10.1136/jnnp.2004.055905

Garde E, Mortensen EL, Krabbe K, Rostrup E, Larsson HB. 2000. Relation between age-related decline in intelligence and cerebral white-matter hyperintensities in healthy octogenarians: a longitudinal study. *Lancet* **356**:628–634. doi:10.1016/S0140-6736(00)02604-0

Genc S, Malpas CB, Gulenc A, Sciberras E, Efron D, Silk TJ, Seal ML. 2020. Longitudinal white matter development in children is associated with puberty, attentional difficulties, and mental health. *bioRxiv*. doi:10.1101/607671

Glasser MF, Sotiropoulos SN, Wilson JA, Coalson TS, Fischl B, Andersson JL, Xu J, Jbabdi S, Webster M, Polimeni JR, Van Essen DC, Jenkinson M. 2013. The minimal preprocessing pipelines for the Human Connectome Project. *Neuroimage* **80**:105–124. doi:10.1016/j.neuroimage.2013.04.127

Gogtay N, Giedd JN, Lusk L, Hayashi KM, Greenstein D, Vaituzis AC, Nugent TF, Herman DH, Clasen LS, Toga AW, Rapoport JL, Thompson PM. 2004. Dynamic mapping of human cortical development during childhood through early adulthood. *Proc Natl Acad Sci U S A* **101**:8174–8179. doi:10.1073/pnas.0402680101

Gorgolewski KJ, Fox AS, Chang L, Schäfer A, Arélin K, Burmann I, Sacher J, Margulies DS. 2014. Tight fitting genes: finding relations between statistical maps and gene expression

patternsF1000Posters. p. 1607 (Poster).

Gorgolewski KJ, Varoquaux G, Rivera G, Schwarz Y, Ghosh SS, Maumet C, Sochat V V., Nichols TE, Poldrack RA, Poline JB, Yarkoni T, Margulies DS. 2015. NeuroVault.Org: A web-based repository for collecting and sharing unthresholded statistical maps of the human brain. *Front Neuroinform* **9**:Article 8. doi:10.3389/fninf.2015.00008

Goulas A, Zilles K, Hilgetag CC. 2018. Cortical Gradients and Laminar Projections in Mammals. *Trends Neurosci* **41**:775–788. doi:10.1016/j.tins.2018.06.003

Graybiel AM. 1995. Building action repertoires: memory and learning functions of the basal ganglia. *Curr Opin Neurobiol* **5**:733–741. doi:10.1016/0959-4388(95)80100-6

Greene AS, Gao S, Scheinost D, Constable RT, Greene A. 2018. Task-induced brain state manipulation improves prediction of individual traits. *Nat Commun* **9**:2807. doi:10.1038/s41467-018-04920-3

Haak K V., Beckmann CF. 2020. Understanding brain organisation in the face of functional heterogeneity and functional multiplicity. *Neuroimage* **220**:117061. doi:10.1016/j.neuroimage.2020.117061

Haak K V., Marquand AF, Beckmann CF. 2018. Connectopic mapping with resting-state fMRI. *Neuroimage* **170**:83–94. doi:10.1016/j.neuroimage.2017.06.075

Hagmann P, Sporns O, Madan N, Cammoun L, Pienaar R, Wedeen VJ, Meuli R, Thiran JP, Grant PE. 2010. White matter maturation reshapes structural connectivity in the late developing human brain. *Proc Natl Acad Sci U S A* **107**:19067–19072. doi:10.1073/pnas.1009073107

Hashimoto R, Ohi K, Yamamori H, Yasuda Y, Fujimoto M, Umeda-Yano S, Watanabe Y, Fukunaga M, Takeda M. 2015. Imaging Genetics and Psychiatric Disorders. *Curr Mol Med* **15**:168–175. doi:10.2174/1566524015666150303104159

Hawrylycz M, Miller JA, Menon V, Feng D, Dolbeare T, Guillozet-Bongaarts AL, Jegga AG, Aronow BJ, Lee CK, Bernard A, Glasser MF, Dierker DL, Menche J, Szafer A, Collman F, Grange P, Berman KA, Mihalas S, Yao Z, Stewart L, Barabási AL, Schulkin J, Phillips J, Ng L, Dang C, R Haynor D, Jones A, Van Essen DC, Koch C, Lein E. 2015. Canonical genetic signatures of the adult human brain. *Nat Neurosci* **18**:1832–1844. doi:10.1038/nn.4171

Hawrylycz MJ, Lein ES, Guillozet-Bongaarts AL, Shen EH, Ng L, Miller JA, van de Lagemaat LN, Smith KA, Ebbert A, Riley ZL, Abajian C, Beckmann CF, Bernard A, Bertagnolli D, Boe AF, Cartagena PM, Mallar Chakravarty M, Chapin M, Chong J, Dalley RA, Daly BD, Dang C, Datta S, Dee N, Dolbeare TA, Faber V, Feng D, Fowler DR, Goldy J, Gregor BW, Haradon Z, Haynor DR, Hohmann JG, Horvath S, Howard RE, Jeromin A, Jochim JM, Kinnunen M, Lau C, Lazarz ET, Lee C, Lemon TA, Li L, Li Y, Morris JA, Overly CC, Parker PD, Parry SE, Reding M, Royall JJ, Schulkin J, Sequeira PA, Slaughterbeck CR, Smith SC, Sodt AJ, Sunkin SM, Swanson BE, Vawter MP, Williams D, Wohnoutka P, Ronald Zielke H, Geschwind DH, Hof PR, Smith SM, Koch C, Grant SGN, Jones AR. 2012. An anatomically comprehensive atlas of the adult human brain transcriptome. *Nature* **489**:391–399. doi:10.1038/nature11405

Herting MM, Johnson C, Mills KL, Vijayakumar N, Dennison M, Liu C, Goddings AL, Dahl RE, Sowell ER, Whittle S, Allen NB, Tamnes CK. 2018. Development of subcortical volumes across adolescence in males and females: A multisample study of longitudinal changes. *Neuroimage* **172**:194–205. doi:10.1016/j.neuroimage.2018.01.020

Hong S-J, Vos De Wael R, Bethlehem RAI, Lariviere S, Paquola C, Valk SL, Milham MP, Martino A Di, Margulies DS, Smallwood J, Bernhardt BC. 2019. Atypical functional connectome

hierarchy in autism. *Nat Commun* **10**:1022.

Hong SJ, Xu T, Nikolaidis A, Smallwood J, Margulies DS, Bernhardt B, Vogelstein J, Milham MP. 2020. Toward a connectivity gradient-based framework for reproducible biomarker discovery. *Neuroimage* **223**:117322. doi:10.1016/j.neuroimage.2020.117322

Huntenburg JM, Bazin PL, Goulas A, Tardif CL, Villringer A, Margulies DS. 2017. A Systematic Relationship Between Functional Connectivity and Intracortical Myelin in the Human Cerebral Cortex. *Cereb cortex* **27**:981–997. doi:10.1093/cercor/bhx030

Huntenburg JM, Bazin PL, Margulies DS. 2018. Large-Scale Gradients in Human Cortical Organization. *Trends Cogn Sci*. doi:10.1016/j.tics.2017.11.002

Hwang K, Bertolero MA, Liu WB, D'Esposito M. 2017. The human thalamus is an integrative hub for functional brain networks. *J Neurosci* **37**:5594–5607. doi:10.1523/JNEUROSCI.0067-17.2017

Ip BK, Wappler I, Peters H, Lindsay S, Clowry GJ, Bayatti N. 2010. Investigating gradients of gene expression involved in early human cortical development. *J Anat* **217**:300–311. doi:10.1111/j.1469-7580.2010.01259.x

Jenkinson M, Beckmann CF, Behrens TEJ, Woolrich MW, Smith SM. 2012. Fsl. *Neuroimage* **62**:782–790. doi:10.1016/j.neuroimage.2011.09.015

Jeurissen B, Tournier JD, Dhollander T, Connelly A, Sijbers J. 2014. Multi-tissue constrained spherical deconvolution for improved analysis of multi-shell diffusion MRI data. *Neuroimage* **103**:411–426. doi:10.1016/j.neuroimage.2014.07.061

Kang HJ, Kawasawa YI, Cheng F, Zhu Y, Xu X, Li M, Sousa AMM, Pletikos M, Meyer KA, Sedmak G, Guennel T, Shin Y, Johnson MB, Krsnik Ž, Mayer S, Fertuzinhos S, Umlauf S, Lisgo SN, Vortmeyer A, Weinberger DR, Mane S, Hyde TM, Huttner A, Reimers M, Kleinman JE, Šestan N. 2011. Spatio-temporal transcriptome of the human brain. *Nature* **478**:483–489. doi:10.1038/nature10523

Kannan SR, Ramathilagam S, Sathya A, Pandiyarajan R. 2010. Effective fuzzy c-means based kernel function in segmenting medical images. *Comput Biol Med* **40**:572–579. doi:10.1016/j.compbiomed.2010.04.001

Khundrakpam BS, Lewis JD, Kostopoulos P, Carbonell F, Evans AC. 2017. Cortical Thickness Abnormalities in Autism Spectrum Disorders Through Late Childhood, Adolescence, and Adulthood: A Large-Scale MRI Study. *Cereb cortex* **27**:1721–1731. doi:10.1093/cercor/bhx038

Khundrakpam BS, Reid A, Brauer J, Carbonell F, Lewis J, Ameis S, Karama S, Lee J, Chen Z, Das S, Evans AC. 2013. Developmental changes in organization of structural brain networks. *Cereb Cortex* **23**:2072–2085. doi:10.1093/cercor/bhs187

Kiddle B, Inkster B, Prabhu G, Moutoussis M, Whitaker KJ, Bullmore ET, Dolan RJ, Fonagy P, Goodyer IM, Jones PB, Dolan R, Hauser T, Vértes P, Whitaker K, Villis L, Bhatti J, Ooi C, Widmer B, Alrumaithi A, Birt S, Cleridou K, Dadabhoy H, Granville S, Harding E, Hopkins A, Isaacs D, King J, Kokorikou D, Mills H, O'Donnell C, Pantaleone S, Dyan P, Fearon P, Kievit R, Stochl J, van Harmelen AL. 2018. Cohort profile: The NSPN 2400 Cohort: A developmental sample supporting the Wellcome Trust Neuro Science in Psychiatry Network. *Int J Epidemiol* **47**:18-19g. doi:10.1093/ije/dyx117

Kilb W. 2012. Development of the GABAergic system from birth to adolescence. *Neuroscientist* **18**:613–630. doi:10.1177/1073858411422114

Klein M, Onnink M, van Donkelaar M, Wolfers T, Harich B, Shi Y, Dammers J, Arias-Vásquez A, Hoogman M, Franke B. 2017. Brain imaging genetics in ADHD and beyond – Mapping pathways from gene to disorder at different levels of complexity. *Neurosci Biobehav Rev* **80**:115–155. doi:10.1016/j.neubiorev.2017.01.013

Koenis MMG, Brouwer RM, Swagerman SC, van Soelen ILC, Boomsma DI, Hulshoff Pol HE. 2018. Association between structural brain network efficiency and intelligence increases during adolescence. *Hum Brain Mapp* **39**:822–836. doi:10.1002/hbm.23885

Kuleshov M V., Jones MR, Rouillard AD, Fernandez NF, Duan Q, Wang Z, Koplev S, Jenkins SL, Jagodnik KM, Lachmann A, McDermott MG, Monteiro CD, Gundersen GW, Ma'ayan A. 2016. Enrichr: a comprehensive gene set enrichment analysis web server 2016 update. *Nucleic Acids Res* **44**:W90–W97. doi:10.1093/nar/gkw377

Lander SS, Linder-Shacham D, Gaisler-Salomon I. 2017. Differential effects of social isolation in adolescent and adult mice on behavior and cortical gene expression. *Behav Brain Res* **316**:245–254. doi:10.1016/j.bbr.2016.09.005

Langs G, Golland P, Ghosh SS. 2015. Predicting Activation Across Individuals with Resting-State Functional Connectivity Based Multi-Atlas Label FusionInternational Conference on Medical Image Computing and Computer-Assisted Intervention. pp. 313–320. doi:10.1007/978-3-319-24571-3_38

Larivière S, Vos de Wael R, Hong S-J, Paquola C, Tavakol S, Lowe AJ, Schrader D V, Bernhardt BC. 2020a. Multiscale Structure–Function Gradients in the Neonatal Connectome. *Cereb Cortex* **30**:47–58. doi:10.1093/cercor/bhz069

Larivière S, Weng Y, Vos de Wael R, Royer J, Frauscher B, Wang Z, Bernasconi A, Bernasconi N, Schrader D V., Zhang Z, Bernhardt BC. 2020b. Functional connectome contractions in temporal lobe epilepsy: Microstructural underpinnings and predictors of surgical outcome. *Epilepsia* **61**:1221–1233. doi:10.1111/epi.16540

Larsen B, Luna B. 2018. Adolescence as a neurobiological critical period for the development of higher-order cognition. *Neurosci Biobehav Rev* **94**:179–195. doi:10.1016/j.neubiorev.2018.09.005

Lebel C, Beaulieu C. 2011. Longitudinal development of human brain wiring continues from childhood into adulthood. *J Neurosci* **31**:10937–10947. doi:10.1523/JNEUROSCI.5302-10.2011

Lee E, Lee J, Kim E. 2017. Excitation/Inhibition Imbalance in Animal Models of Autism Spectrum Disorders. *Biol Psychiatry* **81**:838–847. doi:10.1016/j.biopsych.2016.05.011

Lewis DA, Hashimoto T, Volk DW. 2005. Cortical inhibitory neurons and schizophrenia. *Nat Rev Neurosci* **6**:312–324. doi:10.1038/nrn1648

Liu Y, Zhang LI, Tao HW. 2007. Heterosynaptic scaling of developing GABAergic synapses: Dependence on glutamatergic input and developmental stage. *J Neurosci* **27**:5301–5312. doi:10.1523/JNEUROSCI.0376-07.2007

Lohmann G, Margulies DS, Horstmann A, Pleger B, Lepsien J, Goldhahn D, Schloegl H, Stumvoll M, Villringer A, Turner R. 2010. Eigenvector centrality mapping for analyzing connectivity patterns in fMRI data of the human brain. *PLoS One* **5**:e10232. doi:10.1371/journal.pone.0010232

Louis TA, Robins J, Dockery DW, Spiro A, Ware JH. 1986. Explaining discrepancies between longitudinal and cross-sectional models. *J Chronic Dis* **39**:831–839. doi:10.1016/0021-

9681(86)90085-8

Maier-Hein KH, Neher PF, Houde J-C, Côté M-A, Garyfallidis E, Zhong J, Chamberland M, Yeh F-C, Lin Y-C, Ji Q, Reddick WE, Glass JO, Chen DQ, Feng Y, Gao C, Wu Y, Ma J, He R, Li Q, Westin C-F, Deslauriers-Gauthier S, González JOO, Paquette M, St-Jean S, Girard G, Rheault F, Sidhu J, Tax CMW, Guo F, Mesri HY, Dávid S, Froeling M, Heemskerk AM, Leemans A, Boré A, Pinsard B, Bedetti C, Desrosiers M, Brambati S, Doyon J, Sarica A, Vasta R, Cerasa A, Quattrone A, Yeatman J, Khan AR, Hodges W, Alexander S, Romascano D, Barakovic M, Auría A, Esteban O, Lemkaddem A, Thiran J-P, Cetingul HE, Odry BL, Mailhe B, Nadar MS, Pizzagalli F, Prasad G, Villalon-Reina JE, Galvis J, Thompson PM, Requejo FDS, Laguna PL, Lacerda LM, Barrett R, Dell'Acqua F, Catani M, Petit L, Caruyer E, Daducci A, Dyrby TB, Holland-Letz T, Hilgetag CC, Stieltjes B, Descoteaux M. 2017. The challenge of mapping the human connectome based on diffusion tractography. *Nat Commun* **8**:1349. doi:10.1038/s41467-017-01285-x

Margulies DS, Ghosh SS, Goulas A, Falkiewicz M, Huntenburg JM, Langs G, Bezgin G, Eickhoff SB, Castellanos FX, Petrides M, Jefferies E, Smallwood J. 2016. Situating the default-mode network along a principal gradient of macroscale cortical organization. *Proc Natl Acad Sci U S A* **113**:12574–12579. doi:10.1073/pnas.1608282113

Markello R, Shafiei G, Zheng Y-Q, Mišić B. 2020. abagen: A toolbox for the Allen Brain Atlas genetics data. *Zenodo*. doi:http://doi.org/10.5281/zenodo.4091537

Mars RB, Sotiropoulos SN, Passingham RE, Sallet J, Verhagen L, Khrapitchev AA, Sibson N, Jbabdi S. 2018. Whole brain comparative anatomy using connectivity blueprints. *Elife* **7**:1–15. doi:10.7554/eLife.35237

Marshall WA, Tanner JM. 1970. Variations in the Pattern of Pubertal Changes in Boys. *Arch Dis Child* **45**:13–23. doi:10.1136/adc.45.239.13

Marshall WA, Tanner JM. 1969. Variations in pattern of pubertal changes in girls. *Arch Dis Child* **44**:291–303. doi:10.1136/adc.44.235.291

Mascarell Maričić L, Walter H, Rosenthal A, Ripke S, Quinlan EB, Banaschewski T, Barker GJ, Bokde ALW, Bromberg U, Büchel C, Desrivières S, Flor H, Frouin V, Garavan H, Itterman B, Martinot JL, Martinot MLP, Nees F, Orfanos DP, Paus Tomáš, Poustka L, Hohmann S, Smolka MN, Fröhner JH, Whelan R, Kaminski J, Schumann G, Heinz A, Albrecht L, Andrew C, Arroyo M, Artiges E, Aydin S, Bach C, Banaschewski T, Barbot A, Barker G, Boddaert N, Bokde A, Bricaud Z, Bromberg U, Bruehl R, Cachia A, Cattrell A, Conrod P, Constant P, Dalley J, Decideur B, Desrivieres S, Fadai T, Flor H, Frouin V, Gallinat J, Garavan H, Briand FG, Gowland P, Heinrichs B, Heinz A, Heym N, Hübner T, Ireland J, Ittermann B, Jia T, Lathrop M, Lanzerath D, Lawrence C, Lemaitre H, Lüdemann K, Macare C, Mallik C, Mangin JF, Mann K, Martinot JL, Mennigen E, de Carvahlo FM, Mignon X, Miranda R, Müller K, Nees F, Nymberg C, Paillere ML, Paus Tomas, Pausova Z, Poline JB, Poustka L, Rapp M, Robert G, Reuter J, Rietschel M, Ripke S, Robbins T, Rodehacke S, Rogers J, Romanowski A, Ruggeri B, Schmäl C, Schmidt D, Schneider S, Schumann MG, Schubert F, Schwartz Y, Smolka M, Sommer W, Spanagel R, Speiser C, Spranger T, Stedman A, Steiner S, Stephens D, Strache N, Ströhle A, Struve M, Subramaniam N, Topper L, Walter H, Whelan R, Williams S, Yacubian J, Zilbovicius M, Wong CP, Lubbe S, Martinez-Medina L, Fernandes A, Tahmasebi A. 2020. The IMAGEN study: a decade of imaging genetics in adolescents. *Mol Psychiatry* **25**:2648–2671. doi:10.1038/s41380-020-0822-5

Matarazzo RG, Wiens AN, Matarazzo JD, Manaugh TS. 1973. Test-retest reliability of the WAIS in a normal population. *J Clin Psychol* **29**:194–197. doi:10.1002/1097-4679(197304)29:2<194::AID-JCLP2270290212>3.0.CO;2-W

Meng XL, Rosenthal R, Rubin DB. 1992. Comparing correlated correlation coefficients. *Psychol Bull* **111**:172–175. doi:10.1037/0033-2909.111.1.172

Menon V. 2013. Developmental pathways to functional brain networks: Emerging principles. *Trends Cogn Sci* **17**:627–640. doi:10.1016/j.tics.2013.09.015

Mesulam MM. 1998. From sensation to cognition. *Brain* **121**:1013–1052. doi:10.1093/brain/121.6.1013

Morgan SE, Seidlitz J, Whitaker KJ, Romero-Garcia R, Clifton NE, Scarpazza C, van Amelsvoort T, Marcelis M, van Os J, Donohoe G, Mothersill D, Corvin A, Pocklington A, Raznahan A, McGuire P, Vértes PE, Bullmore ET. 2019. Cortical patterning of abnormal morphometric similarity in psychosis is associated with brain expression of schizophrenia-related genes. *Proc Natl Acad Sci U S A* **116**:9604–9609. doi:10.1073/pnas.1820754116

Müller EJ, Munn B, Hearne LJ, Smith JB, Fulcher B, Arnatkevičiūtė A, Lurie DJ, Cocchi L, Shine JM. 2020. Core and matrix thalamic sub-populations relate to spatio-temporal cortical connectivity gradients. *Neuroimage* **222**:117224. doi:10.1016/j.neuroimage.2020.117224

Murphy C, Wang HT, Konu D, Lowndes R, Margulies DS, Jefferies E, Smallwood J. 2019. Modes of operation: A topographic neural gradient supporting stimulus dependent and independent cognition. *Neuroimage* **186**:487–496. doi:10.1016/j.neuroimage.2018.11.009

Nelson SB, Valakh V. 2015. Excitatory/Inhibitory Balance and Circuit Homeostasis in Autism Spectrum Disorders. *Neuron* **87**:684–698. doi:10.1016/j.neuron.2015.07.033

Oldham S, Fornito A. 2019. The development of brain network hubs. *Dev Cogn Neurosci* **36**:100607. doi:10.1016/j.dcn.2018.12.005

Oligschläger S, Xu T, Baczkowski BM, Falkiewicz M, Falchier A, Linn G, Margulies DS. 2019. Gradients of connectivity distance in the cerebral cortex of the macaque monkey. *Brain Struct Funct* **224**:925–935. doi:10.1007/s00429-018-1811-1

Olson EA, Collins PF, Hooper CJ, Muetzel R, Lim KO, Luciana M. 2009. White matter integrity predicts delay discounting behavior in 9- to 23-year-olds: A diffusion tensor imaging study. *J Cogn Neurosci* **21**:1406–1421. doi:10.1162/jocn.2009.21107

Osmanlıoğlu Y, Tunç B, Parker D, Elliott MA, Baum GL, Ciric R, Satterthwaite TD, Gur RE, Gur RC, Verma R. 2019. System-level matching of structural and functional connectomes in the human brain. *Neuroimage* **199**:93–104. doi:10.1016/j.neuroimage.2019.05.064

Padmanabhan A, Luna B. 2014. Developmental imaging genetics: Linking dopamine function to adolescent behavior. *Brain Cogn* **89**:27–38. doi:10.1016/j.bandc.2013.09.011

Paquola C, Benkarim O, DeKraker J, Larivière S, Frässle S, Royer J, Tavakol S, Valk S, Bernasconi A, Bernasconi N, Khan A, Evans AC, Razi A, Smallwood J, Bernhardt BC. 2020. Convergence of cortical types and functional motifs in the human mesiotemporal lobe. *Elife* **9**:e60673. doi:10.7554/eLife.60673

Paquola C, Bethlehem RA, Seidlitz J, Wagstyl K, Romero-Garcia R, Whitaker KJ, Vos de Wael R, Williams GB, Vértes PE, Margulies DS, Bernhardt B, Bullmore ET. 2019a. Shifts in myeloarchitecture characterise adolescent development of cortical gradients. *Elife* **8**:1–23. doi:10.7554/eLife.50482

Paquola C, Vos De Wael R, Wagstyl K, Bethlehem RAI, Hong SJ, Seidlitz J, Bullmore ET, Evans AC, Misic B, Margulies DS, Smallwood J, Bernhardt BC. 2019b. Microstructural and functional gradients are increasingly dissociated in transmodal cortices. *PLoS Biol*

17:e3000284. doi:10.1371/journal.pbio.3000284

Park B, Byeon K, Park H. 2019. FuNP (Fusion of Neuroimaging Preprocessing) Pipelines: A Fully Automated Preprocessing Software for Functional Magnetic Resonance Imaging. *Front Neuroinform* **13**:5. doi:10.3389/fninf.2019.00005

Park B, Hong J, Lee S-H, Park H. 2016. Functional connectivity of child and adolescent attention deficit hyperactivity disorder patients: Correlation with IQ. *Front Hum Neurosci* **10**. doi:10.3389/fnhum.2016.00565

Park B, Hong S-J, Valk SL, Paquola C, Benkarim O, Bethlehem RAI, Martino A Di, Milham M, Gozzi A, Yeo BTT, Smallwood J, Bernhardt B. 2020a. Connectome and microcircuit models implicate atypical subcortico-cortical interactions in autism pathophysiology. *bioRxiv*. doi:10.1101/2020.05.08.077289

Park B, Park H, Morys F, Kim M, Byeon K, Lee H, Kim S-H, Valk S, Dagher A, Bernhardt BC. 2020b. Body mass variations relate to fractionated functional brain hierarchies. *bioRxiv*. doi:10.1101/2020.08.07.241794

Park B, Vos de Wael R, Paquola C, Larivière S, Benkarim O, Royer J, Tavakol S, Cruces RR, Li Q, Valk SL, Margulies DS, Mišić B, Bzdok D, Smallwood J, Bernhardt BC. 2021. Signal diffusion along connectome gradients and inter-hub routing differentially contribute to dynamic human brain function. *Neuroimage* **224**:117429. doi:10.1016/j.neuroimage.2020.117429

Parvandeh S, Yeh HW, Paulus MP, McKinney BA. 2020. Consensus features nested cross-validation. *Bioinformatics* **36**:3093–3098. doi:10.1093/bioinformatics/btaa046

Patel Y, Parker N, Shin J, Howard D, French L, Thomopoulos SI, Pozzi E, Abe Y, Abé C, Anticevic A, Alda M, Aleman A, Alloza C, Alonso-Lana S, Ameis SH, Anagnostou E, McIntosh AA, Arango C, Arnold PD, Asherson P, Assogna F, Auzias G, Ayesa-Arriola R, Bakker G, Banaj N, Banaschewski T, Bandeira CE, Baranov A, Bargalló N, Bau CHD, Baumeister S, Baune BT, Bellgrove MA, Benedetti F, Bertolino A, Boedhoe PSW, Boks M, Bollettini I, del Mar Bonnin C, Borgers T, Borgwardt S, Brandeis D, Brennan BP, Bruggemann JM, Bülow R, Busatto GF, Calderoni S, Calhoun VD, Calvo R, Canales-Rodríguez EJ, Cannon DM, Carr VJ, Cascella N, Cercignani M, Chaim-Avancini TM, Christakou A, Coghill D, Conzelmann A, Crespo-Facorro B, Cubillo AI, Cullen KR, Cupertino RB, Daly E, Dannlowski U, Davey CG, Denys D, Deruelle C, Di Giorgio A, Dickie EW, Dima D, Dohm K, Ehrlich S, Ely BA, Erwin-Grabner T, Ethofer T, Fair DA, Fallgatter AJ, Faraone S V., Fatjó-Vilas M, Fedor JM, Fitzgerald KD, Ford JM, Frodl T, Fu CHY, Fullerton JM, Gabel MC, Glahn DC, Roberts G, Gogberashvili T, Goikolea JM, Gotlib IH, Goya-Maldonado R, Grabe HJ, Green MJ, Grevet EH, Groenewold NA, Grotegerd D, Gruber O, Gruner P, Guerrero-Pedraza A, Gur RE, Gur RC, Haar S, Haarman BCM, Haavik J, Hahn T, Hajek T, Harrison BJ, Harrison NA, Hartman CA, Whalley HC, Heslenfeld DJ, Hibar DP, Hilland E, Hirano Y, Ho TC, Hoekstra PJ, Hoekstra L, Hohmann S, Hong LE, Höschl C, Høvik MF, Howells FM, Nenadic I, Jalbrzikowski M, James AC, Janssen J, Jaspers-Fayer F, Xu J, Jonassen R, Karkashadze G, King JA, Kircher T, Kirschner M, Koch K, Kochunov P, Kohls G, Konrad K, Krämer B, Krug A, Kuntsi J, Kwon JS, Landén M, Landrø NI, Lazaro L, Lebedeva IS, Leehr EJ, Lera-Miguel S, Lesch K-P, Lochner C, Louza MR, Luna B, Lundervold AJ, MacMaster FP, Maglanoc LA, Malpas CB, Portella MJ, Marsh R, Martyn FM, Mataix-Cols D, Mathalon DH, McCarthy H, McDonald C, McPhilemy G, Meinert S, Menchón JM, Minuzzi L, Mitchell PB, Moreno C, Morgado P, Muratori F, Murphy CM, Murphy D, Mwangi B, Nabulsi L, Nakagawa A, Nakamae T, Namazova L, Narayanaswamy J, Jahanshad N, Nguyen DD, Nicolau R, O'Gorman Tuura RL, O'Hearn K, Oosterlaan J, Opel N, Ophoff

RA, Oranje B, García de la Foz VO, Overs BJ, Paloyelis Y, Pantelis C, Parellada M, Pauli P, Picó-Pérez M, Picon FA, Piras Fabrizio, Piras Federica, Plessen KJ, Pomarol-Clotet E, Preda A, Puig O, Quidé Y, Radua J, Ramos-Quiroga JA, Rasser PE, Rauer L, Reddy J, Redlich R, Reif A, Reneman L, Repple J, Retico A, Richarte V, Richter A, Rosa PGP, Rubia KK, Hashimoto R, Sacchet MD, Salvador R, Santonja J, Sarink K, Sarró S, Satterthwaite TD, Sawa A, Schall U, Schofield PR, Schrantee A, Seitz J, Serpa MH, Setién-Suero E, Shaw P, Shook D, Silk TJ, Sim K, Simon S, Simpson HB, Singh A, Skoch A, Skokauskas N, Soares JC, Soreni N, Soriano-Mas C, Spalletta G, Spaniel F, Lawrie SM, Stern ER, Stewart SE, Takayanagi Y, Temmingh HS, Tolin DF, Tomecek D, Tordesillas-Gutiérrez D, Tosetti M, Uhlmann A, van Amelsvoort T, van der Wee NJA, van der Werff SJA, van Haren NEM, van Wingen GA, Vance A, Vázquez-Bourgon J, Vecchio D, Venkatasubramanian G, Vieta E, Vilarroya O, Vives-Gilabert Y, Voineskos AN, Völzke H, von Polier GG, Walton E, Weickert TW, Weickert CS, Weideman AS, Wittfeld K, Wolf DH, Wu M-J, Yang TT, Yang K, Yoncheva Y, Yun J-Y, Cheng Y, Zanetti M V., Ziegler GC, Franke B, Hoogman M, Buitelaar JK, van Rooij D, Andreassen OA, Ching CRK, Veltman DJ, Schmaal L, Stein DJ, van den Heuvel OA, Turner JA, van Erp TGM, Pausova Z, Thompson PM, Paus T. 2021. Virtual Histology of Cortical Thickness and Shared Neurobiology in 6 Psychiatric Disorders. *JAMA Psychiatry* **78**:47. doi:10.1001/jamapsychiatry.2020.2694

Patenaude B, Smith SM, Kennedy DN, Jenkinson M. 2011. A Bayesian model of shape and appearance for subcortical brain segmentation. *Neuroimage* **56**:907–922. doi:10.1016/j.neuroimage.2011.02.046

Paus T, Keshavan M, Giedd JN. 2008. Why do many psychiatric disorders emerge during adolescence? *Nat Rev Neurosci* **9**:947–957. doi:10.1038/nrn2513

Petanjek Z, Judaš M, Šimić G, Rašin MR, Uylings HBM, Rakic P, Kostović I. 2011. Extraordinary neoteny of synaptic spines in the human prefrontal cortex. *Proc Natl Acad Sci U S A* **108**:13281–13286. doi:10.1073/pnas.1105108108

Ramsden S, Richardson FM, Josse G, Thomas MSC, Ellis C, Shakeshaft C, Seghier ML, Price CJ. 2011. Verbal and non-verbal intelligence changes in the teenage brain. *Nature* **479**:113–116. doi:10.1038/nature10514

Rodríguez-Cruces R, Bernhardt BC, Concha L. 2020. Multidimensional associations between cognition and connectome organization in temporal lobe epilepsy. *Neuroimage* **213**:116706. doi:10.1016/j.neuroimage.2020.116706

Romero-Garcia R, Warrier V, Bullmore ET, Baron-Cohen S, Bethlehem RAI. 2019. Synaptic and transcriptionally downregulated genes are associated with cortical thickness differences in autism. *Mol Psychiatry* **24**:1053–1064. doi:10.1038/s41380-018-0023-7

Romero-Garcia R, Whitaker KJ, Váša F, Seidlitz J, Shinn M, Fonagy P, Dolan RJ, Jones PB, Goodyer IM, Bullmore ET, Vértes PE. 2018. Structural covariance networks are coupled to expression of genes enriched in supragranular layers of the human cortex. *Neuroimage* **171**:256–267. doi:10.1016/j.neuroimage.2017.12.060

Rubinov M, Sporns O. 2010. Complex network measures of brain connectivity: uses and interpretations. *Neuroimage* **52**:1059–1069. doi:10.1016/j.neuroimage.2009.10.003

Sanides F. 1969. Comparative Architectonics of the Neocortex of Mammals and Their Evolutionary Interpretation. *Ann N Y Acad Sci* **167**:404–423. doi:10.1111/j.1749-6632.1969.tb20459.x

Sanides F. 1962. Die Architektonik des Menschlichen Stirnhirns, Monographien aus dem Gesamtgebiete der Neurologie und Psychiatrie. Berlin, Heidelberg: Springer Berlin

Heidelberg. doi:10.1007/978-3-642-86210-6

Schaefer A, Kong R, Gordon EM, Laumann TO, Zuo X-N, Holmes AJ, Eickhoff SB, Yeo BTT. 2018. Local-Global Parcellation of the Human Cerebral Cortex from Intrinsic Functional Connectivity MRI. *Cereb Cortex* **28**:3095–3114. doi:10.1093/cercor/bhx179

Schmithorst VJ, Yuan W. 2010. White matter development during adolescence as shown by diffusion MRI. *Brain Cogn* **72**:16–25. doi:10.1016/j.bandc.2009.06.005

Seidlitz J, Váša F, Shinn M, Romero-Garcia R, Whitaker KJ, Vértes PE, Wagstyl K, Kirkpatrick Reardon P, Clasen L, Liu S, Messinger A, Leopold DA, Fonagy P, Dolan RJ, Jones PB, Goodyer IM, Raznahan A, Bullmore ET. 2018. Morphometric Similarity Networks Detect Microscale Cortical Organization and Predict Inter-Individual Cognitive Variation. *Neuron* **97**:231–247. doi:10.1016/j.neuron.2017.11.039

Shaw P, Greenstein D, Lerch J, Clasen L, Lenroot R, Gogtay N, Evans A, Rapoport J, Giedd J. 2006. Intellectual ability and cortical development in children and adolescents. *Nature* **440**:676–679. doi:10.1038/nature04513

Shin J, French L, Xu T, Leonard G, Perron M, Pike GB, Richer L, Veillette S, Pausova Z, Paus T. 2018. Cell-specific gene-expression profiles and cortical thickness in the human brain. *Cereb Cortex* **28**:3267–3277. doi:10.1093/cercor/bhx197

Shine JM. 2021. The thalamus integrates the macrosystems of the brain to facilitate complex, adaptive brain network dynamics. *Prog Neurobiol* **199**:101951. doi:10.1016/j.pneurobio.2020.101951

Shine JM, Hearne LJ, Breakspear M, Hwang K, Müller EJ, Sporns O, Poldrack RA, Mattingley JB, Cocchi L. 2019. The Low-Dimensional Neural Architecture of Cognitive Complexity Is Related to Activity in Medial Thalamic Nuclei. *Neuron* **104**:849-855.e3. doi:10.1016/j.neuron.2019.09.002

Silveri MM, Sneider JT, Crowley DJ, Covell MJ, Acharya D, Rosso IM, Jensen JE. 2013. Frontal Lobe GABA Levels during Adolescence: Associations with Impulsivity and Response Inhibition. *Biol Psychiatry* **74**:296–304. doi:10.1016/j.biopsych.2013.01.033

Smith RE, Tournier JD, Calamante F, Connelly A. 2015. SIFT2: Enabling dense quantitative assessment of brain white matter connectivity using streamlines tractography. *Neuroimage* **119**:338–351. doi:10.1016/j.neuroimage.2015.06.092

Smith RE, Tournier JD, Calamante F, Connelly A. 2012. Anatomically-constrained tractography: Improved diffusion MRI streamlines tractography through effective use of anatomical information. *Neuroimage* **62**:1924–1938. doi:10.1016/j.neuroimage.2012.06.005

Snow WG, Tierney MC, Zorzitto ML, Fisher RH, Reid DW. 1989. WAIS-R test-retest reliability in a normal elderly sample. *J Clin Exp Neuropsychol* **11**:423–428. doi:10.1080/01688638908400903

Sohal VS, Rubenstein JLR. 2019. Excitation-inhibition balance as a framework for investigating mechanisms in neuropsychiatric disorders. *Mol Psychiatry* **24**:1248–1257. doi:10.1038/s41380-019-0426-0

Sotiras A, Toledo JB, Gur RE, Gur RC, Satterthwaite TD, Davatzikos C. 2017. Patterns of coordinated cortical remodeling during adolescence and their associations with functional specialization and evolutionary expansion. *Proc Natl Acad Sci U S A* **114**:3527–3532. doi:10.1073/pnas.1620928114

Subramanian A, Tamayo P, Mootha VK, Mukherjee S, Ebert BL, Gillette MA, Paulovich A, Pomeroy SL, Golub TR, Lander ES, Mesirov JP. 2005. Gene set enrichment analysis: A knowledge-based approach for interpreting genome-wide expression profiles. *Proc Natl Acad Sci U S A* **102**:15545–15550. doi:10.1073/pnas.0506580102

Suprano I, Kocevar G, Stamile C, Hannoun S, Fourneret P, Revol O, Nusbaum F, Sappey-Marinier D. 2020. White matter microarchitecture and structural network integrity correlate with children intelligence quotient. *Sci Rep* **10**:20722. doi:10.1038/s41598-020-76528-x

Tamnes CK, Herting MM, Goddings AL, Meuwese R, Blakemore SJ, Dahl RE, Güroğlu B, Raznahan A, Sowell ER, Crone EA, Mills KL. 2017. Development of the cerebral cortex across adolescence: A multisample study of inter-related longitudinal changes in cortical volume, surface area, and thickness. *J Neurosci* **37**:3402–3412. doi:10.1523/JNEUROSCI.3302-16.2017

Tamnes CK, Østby Y, Fjell AM, Westlye LT, Due-Tønnessen P, Walhovd KB. 2010. Brain maturation in adolescence and young adulthood: Regional age-related changes in cortical thickness and white matter volume and microstructure. *Cereb Cortex* **20**:534–548. doi:10.1093/cercor/bhp118

Tenenbaum JB, Silva V de, Langford JC. 2000. A Global Geometric Framework for Nonlinear Dimensionality Reduction. *Science (80-)* **290**:2319–2323. doi:10.1126/science.290.5500.2319

Thompson PM, Ge T, Glahn DC, Jahanshad N, Nichols TE. 2013. Genetics of the connectome. *Neuroimage* **80**:475–488. doi:10.1016/j.neuroimage.2013.05.013

Tournier JD, Smith R, Raffelt D, Tabbara R, Dhollander T, Pietsch M, Christiaens D, Jeurissen B, Yeh CH, Connelly A. 2019. MRtrix3: A fast, flexible and open software framework for medical image processing and visualisation. *Neuroimage* **202**:116137. doi:10.1016/j.neuroimage.2019.116137

Trakoshis S, Martínez-Cañada P, Rocchi F, Canella C, You W, Chakrabarti B, Ruigrok ANV, Bullmore ET, Suckling J, Markicevic M, Zerbi V, Baron-Cohen S, Gozzi A, Lai MC, Panzeri S, Lombardo M V. 2020. Intrinsic excitation-inhibition imbalance affects medial prefrontal cortex differently in autistic men versus women. *Elife* **9**:e55684. doi:10.7554/ELIFE.55684

Tziortzi AC, Haber SN, Searle GE, Tsoumpas C, Long CJ, Shotbolt P, Douaud G, Jbabdi S, Behrens TEJ, Rabiner EA, Jenkinson M, Gunn RN. 2014. Connectivity-based functional analysis of dopamine release in the striatum using diffusion-weighted MRI and positron emission tomography. *Cereb Cortex* **24**:1165–1177. doi:10.1093/cercor/bhs397

Valk Sofie L, Kanske P, Park B, Hong S, Raettig AB-, Trautwein F-M, Bernhardt BC, Singer T. 2020. A low-dimensional connectome manifold governs the organization and plasticity of social brain functions in humans. *bioRxiv*. doi:10.1101/2020.11.11.377895

Valk Sofie L., Xu T, Margulies DS, Masouleh SK, Paquola C, Goulas A, Kochunov P, Smallwood J, Yeo BTT, Bernhardt BC, Eickhoff SB. 2020. Shaping brain structure: Genetic and phylogenetic axes of macroscale organization of cortical thickness. *Sci Adv* **6**:1–15. doi:10.1126/sciadv.abb3417

Van Essen DC, Glasser MF, Dierker DL, Harwell J, Coalson T. 2012. Parcellations and hemispheric asymmetries of human cerebral cortex analyzed on surface-based atlases. *Cereb cortex* **22**:2241–2262. doi:10.1093/cercor/bhr291

Varma S, Simon R. 2006. Bias in error estimation when using cross-validation for model selection. *BMC Bioinformatics* **7**:91. doi:10.1186/1471-2105-7-91

Váša F, Romero-Garcia R, Kitzbichler MG, Seidlitz J, Whitaker KJ, Vaghi MM, Kundu P, Patel AX, Fonagy P, Dolan RJ, Jones PB, Goodyer IM, Vértes PE, Bullmore ET. 2020. Conservative and disruptive modes of adolescent change in human brain functional connectivity. *Proc Natl Acad Sci U S A* **117**:3248–3253. doi:10.1073/pnas.1906144117

Vázquez-Rodríguez B, Suárez LE, Markello RD, Shafiei G, Paquola C, Hagmann P, Van Den Heuvel MP, Bernhardt BC, Spreng RN, Misic B. 2019. Gradients of structure–function tethering across neocortex. *Proc Natl Acad Sci U S A* **116**:21219–21227. doi:10.1073/pnas.1903403116

Vértes PE, Rittman T, Whitaker KJ, Romero-Garcia R, Váša F, Kitzbichler MG, Wagstyl K, Fonagy P, Dolan RJ, Jones PB, Goodyer IM, Bullmore ET. 2016. Gene transcription profiles associated with inter-modular hubs and connection distance in human functional magnetic resonance imaging networks. *Philos Trans R Soc B Biol Sci* **371**:20150362. doi:10.1098/rstb.2015.0362

Vos de Wael R, Benkarim O, Paquola C, Lariviere S, Royer J, Tavakol S, Xu T, Hong S-J, Valk SL, Misic B, Milham MP, Margulies DS, Smallwood J, Bernhardt BC. 2020. BrainSpace: a toolbox for the analysis of macroscale gradients in neuroimaging and connectomics datasets. *Commun Biol* **3**:103. doi:10.1038/s42003-020-0794-7

Wagner EE, Caldwell MS. 1979. Wais test-retest reliability for a clinical out-patient sample. *Percept Mot Skills* **48**:131–137. doi:10.2466/pms.1979.48.1.131

Wang P, Kong R, Kong X, Liégeois R, Orban C, Deco G, Van Den Heuvel MP, Yeo BTT. 2019. Inversion of a large-scale circuit model reveals a cortical hierarchy in the dynamic resting human brain. *Sci Adv* **5**:eaat7854. doi:10.1126/sciadv.aat7854

Wechsler D. 1999. Wechsler Abbreviated Scales of Intelligence (WASI). San Antonio, TX: Psychological Corporation.

Weiskopf N, Suckling J, Williams G, Correia M. MM, Inkster B, Tait R, Ooi C, Bullmore T. ET, Lutti A. 2013. Quantitative multi-parameter mapping of R1, PD*, MT, and R2* at 3T: A multi-center validation. *Front Neurosci* **7**:95. doi:10.3389/fnins.2013.00095

Whitaker KJ, Vértes PE, Romero-Garciaa R, Váša F, Moutoussis M, Prabhu G, Weiskopf N, Callaghan MF, Wagstyl K, Rittman T, Tait R, Ooi C, Suckling J, Inkster B, Fonagy P, Dolan RJ, Jones PB, Goodyer IM, Bullmore ET. 2016. Adolescence is associated with genomically patterned consolidation of the hubs of the human brain connectome. *Proc Natl Acad Sci U S A* **113**:9105–9110. doi:10.1073/pnas.1601745113

Wold S, Esbensen K, Geladi P. 1987. Principal component analysis. *Chemom Intell Lab Syst* **2**:37–52. doi:10.1016/0169-7439(87)80084-9

Worsley KJ, Taylor JE, Carbonell, Chung MK, Duerden E, Bernhardt B, Lyttelton O, Boucher M, Evans AC. 2009. SurfStat: A Matlab toolbox for the statistical analysis of univariate and multivariate surface and volumetric data using linear mixed effects models and random field theory. *Neuroimage* **47**:S102. doi:10.1016/S1053-8119(09)70882-1

Xu Q, Guo L, Cheng J, Wang M, Geng Z, Zhu W, Zhang B, Liao W, Qiu S, Zhang H, Xu X, Yu Y, Gao B, Han T, Yao Z, Cui G, Liu F, Qin W, Zhang Q, Li MJ, Liang M, Chen F, Xian J, Li J, Zhang J, Zuo XN, Wang D, Shen W, Miao Y, Yuan F, Lui S, Zhang X, Xu K, Zhang LJ, Ye Z, Yu C. 2020. CHIMGEN: a Chinese imaging genetics cohort to enhance cross-ethnic and cross-geographic brain research. *Mol Psychiatry* **25**:517–529. doi:10.1038/s41380-019-0627-6

Xu T, Nenning KH, Schwartz E, Hong SJ, Vogelstein JT, Goulas A, Fair DA, Schroeder CE,

Margulies DS, Smallwood J, Milham MP, Langs G. 2020. Cross-species functional alignment reveals evolutionary hierarchy within the connectome. *Neuroimage* **223**:117346. doi:10.1016/j.neuroimage.2020.117346

Xu X, Wells AB, O'Brien DR, Nehorai A, Dougherty JD. 2014. Cell type-specific expression analysis to identify putative cellular mechanisms for neurogenetic disorders. *J Neurosci* **34**:1420–1431. doi:10.1523/JNEUROSCI.4488-13.2014

Yarkoni T, Poldrack RA, Nichols TE, Van Essen DC, Wager TD. 2011. Large-scale automated synthesis of human functional neuroimaging data. *Nat Methods* **8**:665–670. doi:10.1038/nmeth.1635

Yeo BTT, Krienen FM, Sepulcre J, Sabuncu MR, Lashkari D, Hollinshead M, Roffman JL, Smoller JW, Zollei L, Polimeni JR, Fischl B, Liu H, Buckner RL. 2011. The organization of the human cerebral cortex estimated by intrinsic functional connectivity. *J Neurophysiol* **106**:1125–1165. doi:10.1152/jn.00338.2011.

Zou H, Hastie T. 2005. Regularization and variable selection via the Elastic Net. *J R Stat Soc Ser B* **67**:301–320. doi:10.1111/j.1467-9868.2005.00503.x

Zuo XN, Ehmke R, Mennes M, Imperati D, Castellanos FX, Sporns O, Milham MP. 2012. Network centrality in the human functional connectome. *Cereb Cortex* **22**:1862–1875. doi:10.1093/cercor/bhr269

Data S1 | Significant gene lists correlated with patterns of manifold eccentricity changes across age. Gene symbol with name and t-statistic as well as false discover rate (FDR) corrected p-value are reported in the Supplementary Data file (Supplementary_Data1.xlsx).

Neuroscience in Psychiatry Network (NSPN) Consortium author list

Principal investigators:
Edward Bullmore (CI from 01/01/2017)[1,2,3]; Raymond Dolan[4,5]; Ian Goodyer (CI until 01/01/2017)[1]; Peter Fonagy[6]; Peter Jones[1]

NSPN (funded) staff:
Michael Moutoussis[4,5]; Tobias Hauser[4,5]; Sharon Neufeld[1]; Rafael Romero-Garcia[1,2]; Michelle St Clair[1]; Petra Vértes[1,2]; Kirstie Whitaker[1,2]; Becky Inkster[1]; Gita Prabhu[4,5]; Cinly Ooi[1]; Umar Toseeb[1]; Barry Widmer[1]; Junaid Bhatti[1]; Laura Villis[1]; Ayesha Alrumaithi[1]; Sarah Birt[1]; Aislinn Bowler[5]; Kalia Cleridou[5]; Hina Dadabhoy[5]; Emma Davies[1]; Ashlyn Firkins[1]; Sian Granville[5]; Elizabeth Harding[5]; Alexandra Hopkins[4,5]; Daniel Isaacs[5]; Janchai King[5]; Danae Kokorikou[5,6]; Christina Maurice[1]; Cleo McIntosh[1]; Jessica Memarzia[1]; Harriet Mills[5]; Ciara O'Donnell[1]; Sara Pantaleone[5]; Jenny Scott[1]; Beatrice Kiddle[1]; Ela Polek[1]

Affiliated scientists:
Pasco Fearon[6]; John Suckling[1]; Anne-Laura van Harmelen[1]; Rogier Kievit[4,7]; Sam Chamberlain[1]

[1]*Department of Psychiatry, University of Cambridge, United Kingdom*
[2]*Behavioural and Clinical Neuroscience Institute, University of Cambridge, United Kingdom*
[3]*ImmunoPsychiatry, GlaxoSmithKline Research and Development, United Kingdom*
[4]*Max Planck University College London Centre for Computational Psychiatry and Ageing Research, University College London, UK*
[5]*Wellcome Centre for Human Neuroimaging, University College London, United Kingdom*
[6]*Research Department of Clinical, Educational and Health Psychology, University College London, United Kingdom*
[7]*Medical Research Council Cognition and Brain Sciences Unit, University of Cambridge, United Kingdom*